July 27, 1972

To the Graduate Council:

I am submitting herewith a dissertation written by Joyce Anne Monard, entitled "Mössbauer Studies of Electrostatic Hyperfine Interactions in ^{238}U, ^{236}U, and ^{234}U." I recommend that it be accepted in partial fulfillment of the requirements for the degree of Doctor of Philosophy, with a major in Physics.

Paul G. Huray
Major Professor

We have read this dissertation
and recommend its acceptance:

John C. Thomson

Joseph R. Peterson

Felix E. Obenshain

Richard L. Becker

T. A. Callcott

Accepted for the Council:

Dean A. Smith
Vice Chancellor for
Graduate Studies and Research

MÖSSBAUER STUDIES OF ELECTROSTATIC HYPERFINE INTERACTIONS IN ^{238}U, ^{236}U, AND ^{234}U

A Dissertation

Presented to

the Graduate Council of

The University of Tennessee

In Partial Fulfillment

of the Requirements for the Degree

Doctor of Philosophy

---

by

Joyce Anne Monard

August 1972

ACKNOWLEDGEMENTS

The author wishes to express her sincere appreciation to the following people who have contributed to this work:

Dr. Paul G. Huray, for suggesting this problem and for guidance in the course of its investigation;

Dr. J.O. Thomson, Dr. F.E. Obenshain, and Dr. M.C. Gregory, for their many useful ideas, suggestions, and discussions;

Dr. O.L. Keller, for the use of the facilities at the Transuranium Research Laboratory;

John E. Bigelow, Leonard C. Williams, and John E. Van Cleve, for preparation of the plutonium dioxide sources;

George W. Parker, for preparation of the uranyl rubidium nitrate absorbers;

James S. Breeden, for his invaluable assistance in a great variety of tasks;

And the National Science Foundation for financial assistance.

1040054

ABSTRACT

The nuclear gamma resonance (NGR) for ^{238}U, ^{236}U, and ^{234}U in the compound $(UO_2)Rb(NO_3)_3$ has been established at 4.2°K following the alpha decay of PuO_2 sources. The ratios of the electric quadrupole moments of these isotopes have been determined and the electric field gradient at the uranium site has been calculated from the data. The isomer shift in ^{234}U has been measured for both PuO_2 and $PuAl_4$ sources and the change in nuclear radius between the excited and the ground state has been calculated.

TABLE OF CONTENTS

CHAPTER		PAGE
I.	INTRODUCTION	1
II.	THEORETICAL CONSIDERATIONS	7
	Multipole Expansion	8
	The Isomer Shift and Relativistic Self-Consistent Field Calculations	17
	Dispersion Effects	19
III.	EXPERIMENTAL DETAILS	24
	Health and Safety Measures	24
	Source Preparation	28
	Absorber Preparation	32
	Mössbauer Spectrometer	34
	Calibration	44
	Data Analysis	45
IV.	EXPERIMENTAL RESULTS AND DISCUSSION	48
	Solid State Properties of Sources and Absorbers	48
	Comparative Mössbauer Results for ^{238}U, ^{236}U, and ^{234}U	55
	Comparative Mössbauer Results for ^{234}U	64
	Conclusions	71
LIST OF REFERENCES		72
APPENDICES		77
A.	HIGH-VELOCITY COIL	78
B.	FOURIER ANALYSIS OF CALIBRATION SPECTRA	83
C.	CONVERSION FROM CHANNELS TO VELOCITY	86
VITA		88

LIST OF TABLES

TABLE		PAGE
I.	Nuclear Properties of Sources and Absorbers.	6
II.	Relativistic Values of the Electron Probability Density at the Nucleus for ^{234}U.	20
III.	Permissible Doses for Internal Radiation	25
IV.	Physical Properties of Plutonium Sources	29
V.	Physical Properties of Uranium Absorbers	33
VI.	Experimental Details of Mössbauer Runs	41
VII.	Measured Mössbauer Parameters for PuO_2 Sources Versus $(UO_2)Rb(NO_3)_3$ Absorbers.	60
VIII.	Measured Mössbauer Parameters for $^{238}PuO_2$ and $^{238}PuAl_4$ Sources Versus $(^{234}UO_2)Rb(NO_3)_3$ Absorbers.	67
IX.	Velocity Coil Dimensions	80
X.	Velocity Coil Windings	81
XI.	Actual Windings for High-Velocity Coil	82

LIST OF FIGURES

FIGURE PAGE

1. Decay Schemes and Nuclear Energy Levels for the ^{234}U, ^{236}U, and ^{238}U Mössbauer Nuclei. 4
2. Interaction Between Nuclear Charge Density (ρ_N, $d\tau_N$) and Electronic Charge Density (ρ_E, $d\tau_E$). 9
3. Splitting of the 2^+ State in ^{234}U, ^{236}U, or ^{238}U Due to the Electrostatic Hyperfine Structure Coupling 16
4. Changes in the Relativistic Electron Probability Density at the Nucleus with the Oxidation States of ^{234}U. 21
5. Safety Features of the Transuranium Research Laboratory. 27
6. Schematic of the Source Container. 30
7. Schematic of the Cryostat. 35
8. Block Diagram of the Initial Electronic Configuration. 38
9. Circuit Diagram of the Crystal Oscillator. 40
10. Block Diagram of the Revised Electronic Configuration. 43
11. Atomic Arrangement in Uranyl Rubidium Nitrate. 49
12. Structure of the Uranyl Rubidium Nitrate Molecule. 51
13. The Fluorite Structure Formed by PuO_2. 52
14. The Structure of $PuAl_4$ 54
15. Mössbauer Spectrum of ^{238}U in $(UO_2)Rb(NO_3)_3$ Following the Alpha Decay of ^{242}Pu in PuO_2 at 4.2° K 56
16. Mössbauer Spectrum of ^{236}U in $(UO_2)Rb(NO_3)_3$ Following the Alpha Decay of ^{240}Pu in PuO_2 at 4.2° K 57
17. Mössbauer Spectrum of ^{234}U in $(UO_2)Rb(NO_3)_3$ Following the Alpha Decay of ^{238}Pu in PuO_2 at 4.2° K 58

FIGURE PAGE

18. Mössbauer Spectrum of ^{234}U in $(UO_2)Rb(NO_3)_3$ Following the Alpha Decay of ^{238}Pu in $PuAl_4$ at 4.2° K. 65

19. Mössbauer Spectrum of ^{234}U in $(UO_2)Rb(NO_3)_3$ Following the Alpha Decay of ^{238}Pu in PuO_2 at 4.2° K 66

20. Schematic of the Velocity Coilform 79

CHAPTER I

INTRODUCTION

The even-even isotopes of the actinide elements (atomic numbers 90 to 103) lie in the second region of deformed nuclei where the lowest nuclear levels are collective in nature with rather small excitation energies. Little is known about the solid state properties of these elements because of their scarcity and radioactivity. The chemical properties of the actinides have been studied somewhat more extensively, and it has been shown that these elements (especially the lighter members of the series) form a multiplicity of stable oxidation states. It is well known that the actinides form a transition series due to the filling of the 5f electron shell, analogous to the rare-earth series in which the 4f shell is filled. Since the gamma transition from the 2^+ first excited state to the 0^+ ground state in the even-even actinide nuclei has been recognized for several years as a possible Mössbauer candidate,[1] the Mössbauer technique may become a valuable probe into the nuclear and solid state properties of these elements.

R.L. Mössbauer pointed out in 1957 that under proper conditions the lattice as a whole can absorb the recoil momentum following a low energy gamma transition and the nucleus can emit without recoil a gamma ray with the full transition energy.[2] For gamma-ray transitions with lifetimes of the order of nanoseconds the natural linewidth is frequently less than or comparable to the nuclear hyperfine interaction energies. In such cases, the hyperfine splitting of nuclear levels may be resolved by measuring the change in nuclear gamma-ray absorption as a function of

Doppler velocity between a recoilless emitter (source) and a recoilless absorber. However, the utility of the Mössbauer effect goes beyond the measurement of nuclear parameters, for it also provides a means of investigating magnetic behaviour, crystal field effects, and other solid state properties.[3]

Mössbauer spectroscopy is most often performed using the beta decay or electron capture of radioactive sources to populate the excited states. It is usually desirable to choose a source which produces gamma rays from nuclear states unsplit by hyperfine interactions. Then an absorber whose nuclear levels are split by hyperfine interactions may be studied by Doppler shifting the source gamma rays with respect to the absorber gamma rays in a regular, reproducible manner and detecting the transmitted or scattered gamma rays as a function of the Doppler velocity. Coulomb excitation may also be used to excite the level of interest in a Mössbauer nucleus.[4]

The predominant mode of decay in the even-even actinides is by the emission of alpha particles. There has been some question in the past as to the effect that nuclear recoil and/or radiation damage in the source may have on Mössbauer spectra, whether the excited state is reached by Coulomb excitation, as in the earliest even-even actinide experiments,[5] or by alpha decay.[6] Several questions arise concerning the manner in which a nucleus comes to rest in the lattice after Coulomb excitation. It is necessary to know whether the recoiling excited nucleus becomes bound again in the lattice in a time short compared to the lifetime of the excited nuclear state, whether the emitting nucleus is bound in a normal lattice site, and whether the recoil energy is locally distributed. Results in the rare earths[7] indicate that radiation damage to the lattice

due to incident particles is not significant for the Mössbauer effect. Results show that the recoiling nucleus may come to rest in a normal lattice position and have nearly the same probability of recoilless emission as a nuclear transition reached by beta decay. The recoil energy of the residual nucleus after alpha decay is sufficient to remove the recoiling atom from its lattice site and to disrupt the local crystalline binding forces; however, it has been shown experimentally that the Mössbauer effect can be observed after alpha decay.[6]

This dissertation presents the results of Mössbauer measurements of the electric hyperfine interactions of the 2^+ to 0^+ transition in ^{238}U, ^{236}U, and ^{234}U. The alpha decay of the plutonium parents was used to populate the first excited state of the uranium isotopes. The decay schemes are shown in Figure 1. The special nature of these actinide elements leads to complicating factors which do not occur in other Mössbauer experiments. Ordinarily, one desires a stable element from which to fabricate an absorber; however, all of the uranium isotopes are radioactive (see Figure 1). The absorber radioactivity produces a complication since it provides unwanted background. Nevertheless, the half-life of the uranium absorber is long compared with the half-life of the plutonium source and the length of the experiment, and hence may be considered effectively stable. A further complication is that high isotopic purities (for both sources and absorbers) are required for successful experiments. Such isotopes are expensive, scarce, and require careful handling since they are extremely toxic and constitute a possible hazard in the laboratory. One last difficulty to be noted is the fact that the large internal conversion coefficients of the 45 keV resonant gamma rays will seriously decrease the source gamma-ray intensity and the resonant absorption cross

ORNL-DWG 72-287

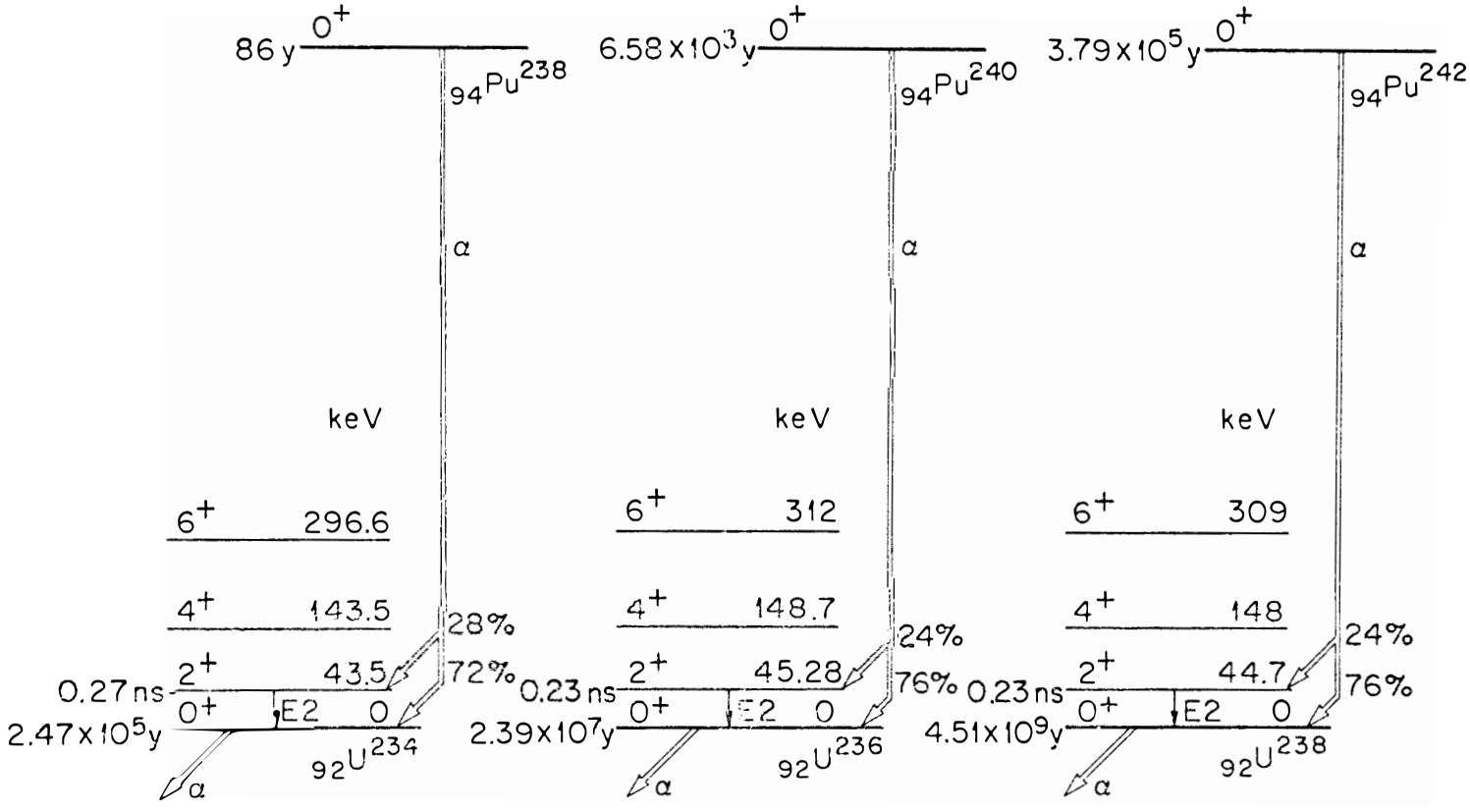

Figure 1. Decay schemes and nuclear energy levels for the ^{234}U, ^{236}U, and ^{238}U Mössbauer nuclei.

section. Some nuclear properties of sources and absorbers are listed in Table I.

In this study, measurements have been made of the quadrupole coupling constants in ^{238}U, ^{236}U, and ^{234}U. From the data, the ratios of the quadrupole moments of these isotopes have been determined and the electric field gradient at the uranium site in the uranyl rubidium nitrate $[(UO_2)Rb(NO_3)_3]$ absorber has been calculated. Preliminary reports of this work have been published.[8,9] An extensive Mössbauer study of the isotope ^{238}U has been published by S.L. Ruby, et al.[10] and a study of all three isotopes has been reported by R. Meeker, et al.[11] Also discussed in this dissertation are the isomer shift in ^{234}U, which has been measured for PuO_2 and $PuAl_4$ sources, and the possibility of an interference effect between the Mössbauer gamma rays and the internal conversion electrons.[12]

Table I

Nuclear Properties of Sources and Absorbers

Absorber	Energy of 2^+ Excited State (keV)[a]	Lifetime of 2^+ Excited State (nsec)[b]	Internal Conversion Coefficient[c]	Intrinsic Quadrupole Moment (barns)[a]	Energy of Alpha Decay Which Populates the 2^+ State (MeV)[b]	Source
^{234}U	43.491 ± 0.009	0.27	635	10.19 ± 0.13	5.456	^{238}Pu
^{236}U	45.242 ± 0.006	0.23	612	10.81 ± 0.11	5.123	^{240}Pu
^{238}U	44.915 ± 0.013	0.23	746	10.84 ± 0.07	4.863	^{242}Pu

[a] J.L.C. Ford, Jr., P.H. Stelson, C.E. Bemis, Jr., F.K. McGowan, R.L. Robinson, and W.T. Milner, Phys. Rev. Letters 27, 1232 (1971).

[b] C.M. Lederer, J.M. Hollander, and I. Perlman, Table of Isotopes, (John Wiley and Sons, Inc., New York, 1967), 6th ed.

[c] M. Schmorak, C.E. Bemis, Jr., M.J. Zender, N.B. Gove, and P.F. Dittner, Nucl Phys. A178, 410 (1972).

CHAPTER II

THEORETICAL CONSIDERATIONS

The interaction of the nucleus with the atomic electrons normally gives rise to both electrostatic and magnetic hyperfine structure. The perturbation of the nuclear energy levels by these hyperfine interactions splits the nuclear spin degeneracy, and in general destroys the nuclear gamma resonance condition for the case of no relative motion between the source and absorber. However, resonance for each component may be restored by imparting a Doppler velocity, v, to the emitting or absorbing nucleus. The change in energy, ΔE, of the modulated gamma ray of energy E_γ is given by:

$$\Delta E = E_\gamma v/c \tag{1}$$

where c is the speed of light. Doppler velocities here will be considered positive when the absorber is approaching the source.

The sources and absorbers used in this work are believed to be non-magnetic,[13] and the Mössbauer spectra observed substantiate this statement. For this reason, the magnetic hyperfine interaction will be neglected in the following treatment. The perturbation of the nuclear energy levels by the surrounding electrons in the solid can be described by a multipole expansion. The odd terms in this expansion vanish if the nuclear state is an eigenfunction of parity[14] and only the lowest three even terms (monopole, quadrupole, and hexadecapole) are expected to make a measurable contribution to the hyperfine interaction. In the following, quantum mechanical Hamiltonian operators will be represented by $\hat{H}$ and their expectation values by H.

I. MULTIPOLE EXPANSION

Let us consider a nucleus under the action of an electrostatic field. The interaction energy between the nuclear and electronic charge densities is given classically by:[14]

$$H_{elec} = \int_E \int_N \frac{\rho_E(\vec{r}_E)\rho_N(\vec{r}_N)d\tau_E d\tau_N}{|\vec{r}_E - \vec{r}_N|} \tag{2}$$

where $\rho_E(\vec{r}_E)$ and $\rho_N(\vec{r}_N)$ are the electronic and nuclear charge densities, respectively. The symbols $\vec{r}_E$, $\vec{r}_N$, $d\tau_E$, and $d\tau_N$ are defined schematically in Figure 2. The term $1/|\vec{r}_E - \vec{r}_N|$ can be expanded in spherical harmonics:

$$\frac{1}{|\vec{r}_E - \vec{r}_N|} = \sum_{\ell=0}^{\infty} \sum_{m=-\ell}^{\ell} \frac{4\pi}{2\ell + 1} \frac{r_<^{\ell}}{r_>^{\ell+1}} Y_{\ell m}(\theta_N,\phi_N) Y^*_{\ell m}(\theta_E,\phi_E) \tag{3}$$

where $r_<$ and $r_>$ signify the smaller and larger of the magnitudes of the two radius vectors $\vec{r}_E$ and $\vec{r}_N$, and the $Y_{\ell m}(\theta,\phi)$ are the normalized spherical harmonics of the nuclear (subscript N) or electronic (subscript E) coordinates. The terms $r_E < r_N$ arise from electron penetration of the nucleus.

The monopole interaction is the term of Equations (2) and (3) for which $\ell = 0$ and is given by:

$$H_{mon} = 4\pi \int_E \int_N \frac{\rho_E(\vec{r}_E)\rho_N(\vec{r}_N)d\tau_E d\tau_N}{r_>} . \tag{4}$$

Under the assumptions that the electronic charge density is uniform over the nuclear dimensions and that the potential outside the nucleus is independent of the nuclear charge distribution, it may be shown that:[15]

ORNL-DWG 72-7412

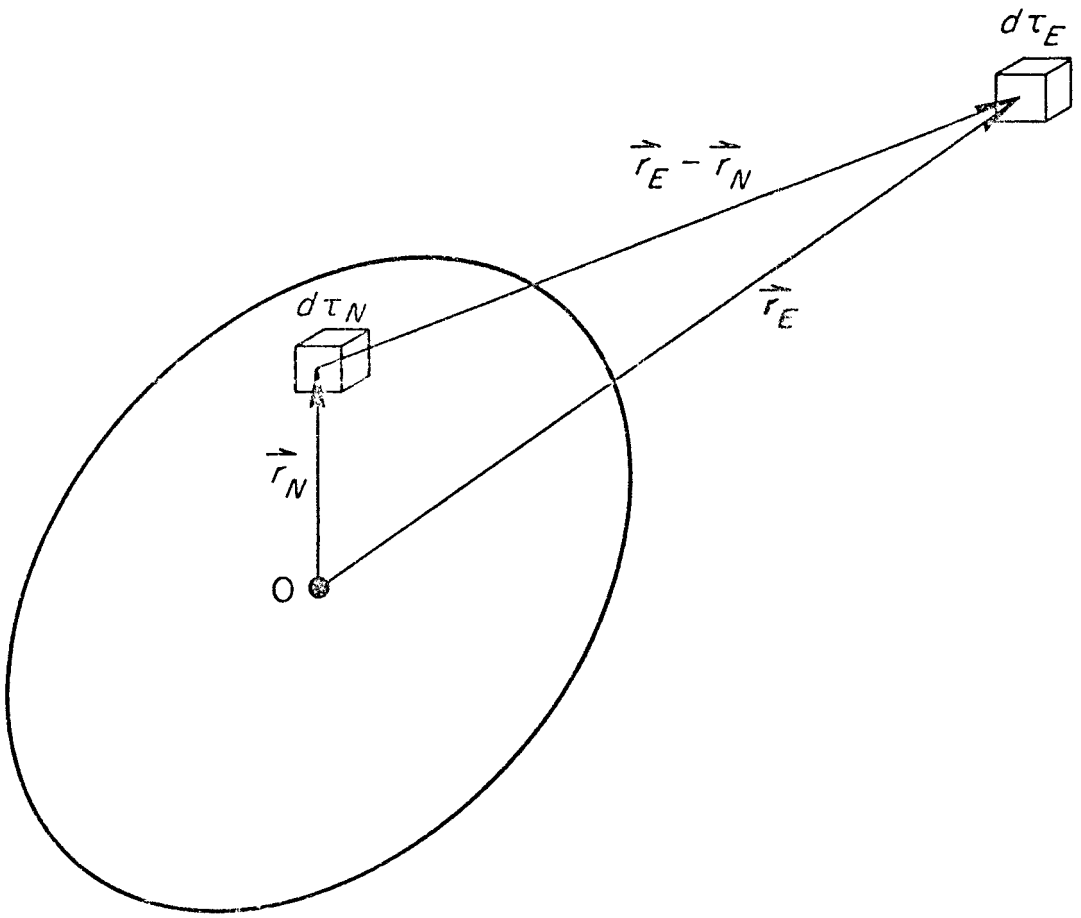

Figure 2. Interaction between nuclear charge density (ρ_N, $d\tau_N$) and electronic charge density (ρ_E, $d\tau_E$).

$$H_{mon} \simeq ZeV + \frac{2\pi}{3} Ze^2 < r_N^2 > |\psi(0)|^2 \tag{5}$$

where

$$Ze \simeq \int_N \rho_N(\vec{r}_N) d\tau_N, \tag{6}$$

$$V \simeq \int_E \frac{\rho_E(\vec{r}_E)}{r_E} d\tau_E, \tag{7}$$

$$Ze <r_N^2> \simeq \int_N r_N^2 \rho_N(\vec{r}_N) d\tau_N, \tag{8}$$

and $|\psi(0)|^2$ is the electron probability density averaged over the nucleus. The electronic charge density is related to the electron probability density by:

$$\rho'_E(r_E) = -e|\psi(r_E)|^2. \tag{9}$$

Here,

$$\rho'_E(r_E) = \frac{1}{4\pi} \int\int \rho_E(\vec{r}_E) \sin \theta_E \, d\theta_E \, d\phi_E, \tag{10}$$

and is the electronic charge density averaged over a sphere of radius r_E. The first term in Equation (5) is the Coulomb energy for a point nucleus. The second term in Equation (5) is the energy shift (δ) due to the fact that the electrons have a finite charge density within the nuclear volume, or

$$\delta \simeq \frac{2\pi}{3} Ze^2 <r_N^2> |\psi(0)|^2. \tag{11}$$

The Mössbauer gamma-ray energy, E_γ, depends on the difference in the electrostatic energy of the nucleus in two different states. Therefore, E_γ differs from that energy which would be expected for a point nucleus undergoing a transition from an excited (ex) to a ground (gr) state by:

$$\delta_{ex} - \delta_{gr} = \frac{2\pi}{3} Ze^2(\langle r_N^2\rangle_{ex} - \langle r_N^2\rangle_{gr})|\psi(0)|^2. \tag{12}$$

The isomer shift measured in Mössbauer spectroscopy arises from a difference in the electronic charge density at the source and absorber nuclei. This will be discussed in the next section.

The contribution to the hyperfine interaction for $r_E<r_N$ is significant for the monopole term; however, we shall ignore the electron penetration into the nucleus for higher order terms. For $r_E>r_N$ the electrostatic interaction energy of Equations (2) and (3) may be factored to give:

$$H_{elec} \simeq \sum_{\ell=0}^{\infty} \sum_{m=-\ell}^{\ell} N_{\ell m} E^*_{\ell m} \tag{13}$$

where

$$N_{\ell m} = \sqrt{\frac{4\pi}{2\ell+1}} \int_N r_N^{\ell} \rho_N(\vec{r}_N) Y_{\ell m}(\theta_N, \phi_N) d\tau_N \tag{14}$$

and

$$E^*_{\ell m} = \sqrt{\frac{4\pi}{2\ell+1}} \int_E \frac{\rho_E(\vec{r}_E)}{r_E^{\ell+1}} Y^*_{\ell m}(\theta_E, \phi_E) d\tau_E. \tag{15}$$

As mentioned above, terms with odd values of ℓ are omitted because the nuclear wave functions are thought to be eigenstates of parity.[14] The series is rapidly convergent because successive terms (with even ℓ values) decrease as (nuclear radius/electronic radius)^2 or approximately as

$(10^{-12}\text{cm}/10^{-8}\text{cm})^2$ or 10^{-8}. Terms beyond the quadrupole term, for example the hexadecapole term, have been detected experimentally only in rare cases.[16,17]

The quadrupole interaction is the term of Equations (13), (14), and (15) for which $\ell = 2$ and is given by:

$$H_{quad} \simeq \frac{4\pi}{5} \sum_{m=-2}^{+2} [\int_N r_N^2 \rho_N(\vec{r}_N) Y_{2m}(\theta_N, \phi_N) d\tau_N] \tag{16}$$

$$\times [\int_E \frac{\rho_E(\vec{r}_E)}{r_E^3} Y_{2m}^*(\theta_E, \phi_E) d\tau_E].$$

By application of the Wigner-Eckart theorem and substitution of the appropriate Clebsch-Gordan coefficients, it can be shown that the quadrupole term arises from the interaction between the nuclear quadrupole moment, Q, and the second derivative of the potential, $q \equiv \partial^2 V/\partial z^2$. The quantum mechanical Hamiltonian operator is given by:[14]

$$\hat{H}_{quad} = \frac{eqQ}{4I(2I-1)} [(3\hat{I}_z^2 - \hat{I}^2) + \tfrac{1}{2}\eta(\hat{I}_+^2 + \hat{I}_-^2)] \tag{17}$$

where

$$eQ \equiv \int_N \psi^*_{I,I_z=I} r_N^2 \rho_N(\vec{r}_N)(3\cos^2\theta_N - 1)\psi_{I,I_z=I} d\tau_N \tag{18}$$

and

$$q \equiv \int_E \frac{\rho_E(\vec{r}_E)}{r_E^3} (3\cos^2\theta_E - 1) d\tau_E \equiv \frac{-\partial E_z}{\partial z} . \tag{19}$$

Here, $\hat{I}$, $\hat{I}_z$, $\hat{I}_+$, and $\hat{I}_-$ are the nuclear angular momentum operators,[18] ψ is the nuclear wave function, and η, the asymmetry parameter, is given by:

$$\eta \equiv (\frac{\partial^2 V}{\partial x^2} - \frac{\partial^2 V}{\partial y^2}) / (\frac{\partial^2 V}{\partial z^2}). \tag{20}$$

By convention, the x, y, and z axes are selected so that:

$$\left|\frac{\partial^2 V}{\partial z^2}\right| \geq \left|\frac{\partial^2 V}{\partial x^2}\right| \geq \left|\frac{\partial^2 V}{\partial y^2}\right|, \tag{21}$$

and η will take on values between zero and unity. In our absorber compound, uranyl rubidium nitrate, the high degree of crystalline axial symmetry allows us to assume that η is equal to zero (see Chapter IV). Equation (17) thus simplifies to the form:

$$\hat{H}_{quad} = \frac{eqQ}{4I(2I - 1)} (3\hat{I}_z^2 - \hat{I}^2) \quad . \tag{22}$$

The degeneracy of the nuclear spin states has not been completely removed, since levels with $\pm I_z$ have the same energy.

It should be noted that Q is the spectroscopic quadrupole moment and not the intrinsic quadrupole moment Q_o. They are related in the strong coupling model by the product of two Clebsch-Gordan coefficients:[19]

$$Q = Q_o \langle I2I_z0 | II_z \rangle \langle I2K0 | IK \rangle \Big|_{I_z=I} \tag{23}$$

where K is the component of the angular momentum vector $\vec{I}$ along the symmetry axis of the body frame. Substituting for the Clebsch-Gordan coefficients:

$$Q = Q_o \left. \frac{[3I_z^2 - I(I + 1)][3K^2 - I(I + 1)]}{I(I + 1)(2I - 1)(2I + 3)} \right|_{I_z=I} . \tag{24}$$

The spectroscopic quadrupole moment vanishes for $I<1$, thus the quadrupole interaction may only be observed for nuclear spin states with $I \geq 1$.

The hexadecapole interaction is the term of Equations (13), (14), and (15) for which $\ell = 4$ and is given by:

$$H_{hex} = \frac{4\pi}{9} \sum_{m=-4}^{+4} [\int_N r_N^4 \rho_N(\vec{r}_N) Y_{4m}(\theta_N, \phi_N) d\tau_N] \tag{25}$$

$$\times [\int_E \frac{\rho_E(\vec{r}_E)}{r_E^5} Y^*_{4m}(\theta_E, \phi_E) d\tau_E].$$

By application of the Wigner-Eckart theorem and substitution of the appropriate Clebsch-Gordan coefficients, it can be shown that the hexadecapole term arises from the interaction between the nuclear hexadecapole moment, M, and the fourth derivative of the potential, $m \equiv \partial^4 V/\partial z^4$. With the assumption of axial symmetry, the quantum mechanical Hamiltonian operator is given by:[16]

$$\hat{H}_{hex} = \frac{emM[35\hat{I}_z^4 - 30\hat{I}_z^2\hat{I}^2 + 3\hat{I}^4 + 25\hat{I}_z^2 - 6\hat{I}^2]}{128I(I-1)(2I-1)(2I-3)} \tag{26}$$

where

$$eM \equiv \int_N \psi_{I,I_z=I} r_N^4 \rho_N(\vec{r}_N)(35\cos^4\theta_N - 30\cos^2\theta_N + 3)\psi_{I,I_z=I} d\tau_N \tag{27}$$

and

$$m \equiv \int_E \frac{\rho_E(\vec{r}_E)}{r_E^5} (35\cos^4\theta_E - 30\cos^2\theta_E + 3) d\tau_E \equiv \frac{-\partial^3 E_z}{\partial z^3} . \tag{28}$$

Nuclear spin states of $\pm I_z$ are still degenerate, as in the quadrupole case.

The quantity M is the spectroscopic hexadecapole moment and is related to the intrinsic hexadecapole moment M_o in the strong coupling model by the product of two Clebsch-Gordan coefficients:

$$M = M_o \langle I4I_z0|II_z\rangle \langle I4K0|1K\rangle \Big|_{I_z=I} \tag{29}$$

$$= 4M_o \frac{[35I_z^4 - 30I_z^2 I(I+1) + 25I_z^2 - 6I(I+1) + 3I^2(I+1)^2]}{(2I+5)(2I+4)(2I+3)(2I+2)(2I)(2I-1)(2I-2)(2I-3)} \tag{30}$$

$$\times [35K^4 - 30K^2 I(I+1) + 25K^2 - 6I(I+1) + 3I^2(I+1)^2]\Big|_{I_z=I} .$$

The spectroscopic hexadecapole moment vanishes for $I<2$, thus the hexadecapole interaction may only be observed for nuclear spin states with $I \geq 2$.

The multipole expansion shows that each electrostatic hyperfine interaction is the product of a nuclear parameter (Ze for the Coulomb energy, $Ze\langle r_N^2\rangle$ for the energy shift, eQ for the quadrupole interaction, and eM for the hexadecapole interaction) and a solid state parameter (V for the Coulomb energy, $|\psi(0)|^2$ for the energy shift, q for the quadrupole interaction, and m for the hexadecapole interaction). The level splittings for these interactions for the 2^+ to 0^+ transition in the three uranium isotopes are shown in Figure 3. If the interaction contains only monopole and quadrupole terms (with η equal to zero), the ratio of the splittings between the levels will be 3:1. If the hexadecapole interaction is present, the splitting ratio will be different from 3:1.

The relative intensities of the absorption lines will be proportional to the transition probabilities between the initial and final states of the nucleus and the relative populations of the initial states. For the temperature used in this set of experiments (4.2°K), the populations of the initial states are approximately equal and the transition probabilities are a function only of the angular momentum L associated

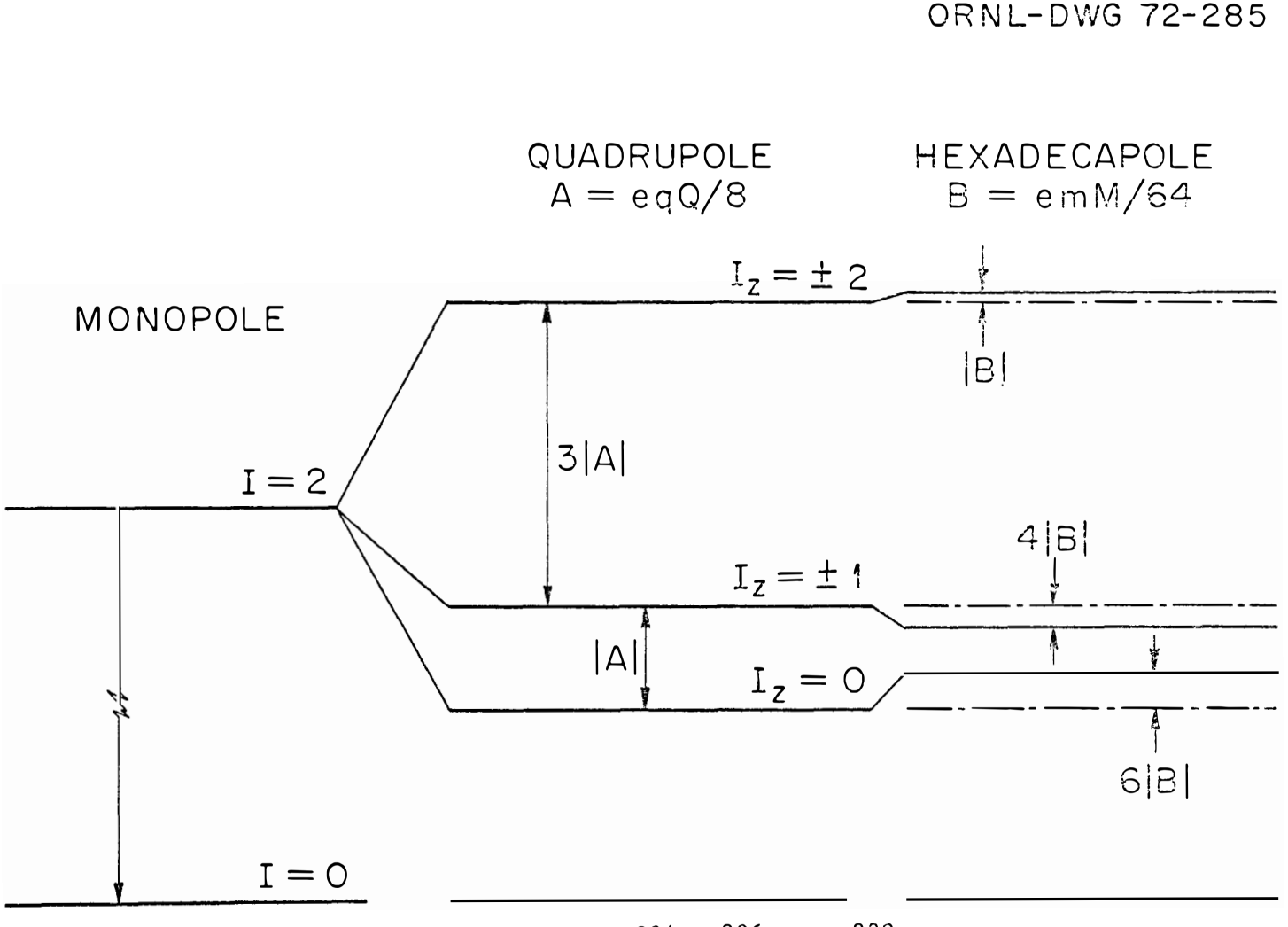

Figure 3. Splitting of the 2^+ state in ^{234}U, ^{236}U, or ^{238}U due to the electrostatic hyperfine structure coupling.

with the radiation field and ΔI_z the change in projection quantum number between the initial and final states. For an assembly of randomly oriented nuclei (powdered sample), the relative transition probability will be equal to the square of the Clebsch-Gordan coefficient $\langle I_{gr} L I_{z_{gr}} (I_{z_{ex}} - I_{z_{gr}}) | I_{ex} I_{z_{ex}} \rangle$.[20] Thus for the transitions $\Delta I_z = \pm 2$, $\Delta I_z = \pm 1$, and $\Delta I_z = 0$, the relative probabilities are 2, 2, and 1, respecively. If the Debye-Waller factor depends on the direction of gamma-ray emission with respect to the crystal axes, then the relative intensities will differ from these values.[21]

II. THE ISOMER SHIFT AND RELATIVISTIC SELF-CONSISTENT FIELD CALCULATIONS

The energy shift for transitions between the excited and the ground states given in Equation (12) is a correction term which arises from the penetration of the atomic electrons into the finite nucleus. For simplicity, the nuclear charge distribution will be taken as uniform for $r<R$, the "equivalent" nuclear radius, and as zero for $r>R$. Thus, equations will be given which, when compared with experimental data, yield the fractional change in charge radius, $\Delta R/R$, of the uniform charge distribution. However, the uniform charge distribution is "equivalent" to the true charge distribution of the real isomeric states. The "equivalent" radius is related to the mean-square radius by:[19]

$$R^2 = \frac{5}{3} \langle r_N^2 \rangle, \tag{31}$$

and therefore Equation (12) may be rewritten:

$$\delta_{ex} - \delta_{gr} = \frac{2\pi}{5} Ze^2(R^2_{ex} - R^2_{gr})|\psi(0)|^2. \tag{32}$$

Only the s electrons have been found to contribute significantly to the value of $|\psi(0)|^2$ in the non-relativistic approximation; however, the $p_{1/2}$ electrons also have a small but finite amplitude at the origin if relativistic effects are taken into account.

If the electronic charge density at the absorbing nuclei (subscript A) is different from that of the emitting nuclei (subscript S), then the centroid of the experimental resonance will be shifted from zero relative velocity. The experimental isomer shift, δ_{IS}, in velocity units is given by:[22]

$$\delta_{IS} = \frac{2\pi}{5} Ze^2\frac{c}{E_\gamma}(R^2_{ex} - R^2_{gr})(|\psi_A(0)|^2 - |\psi_S(0)|^2) \tag{33}$$

$$= \frac{4\pi}{5} Ze^2\frac{c}{E_\gamma}\frac{\Delta R}{R} R^2(|\psi_A(0)|^2 - |\psi_S(0)|^2) .$$

The relation $\Delta(R^2) = 2R\Delta R = 2R^2\Delta R/R$ has been used to obtain the second form of Equation (33) where $\Delta R = R_{ex} - R_{gr}$. A positive δ_{IS} corresponds to a shift of the absorption resonance to a higher energy than that of the source.

In order to obtain estimates of the fractional change in charge radius between the excited and the ground states of the Mössbauer nucleus, it is necessary to calculate the electronic charge density in the source and absorber. A series of computer programs is in operation at the Oak Ridge National Laboratory which provides calculations of relativistic Hartree-Fock-Slater wave functions[23] for atoms and ions which are free or

have Wigner-Seitz boundary conditions. The electron probability densities were calculated using the computer code NEWREL. This program is capable of computing relativistic and nonrelativistic self-consistent field wave functions with Slater-Latter exchange potential for free atoms and ions. Binding energies, mean radii, screening constants, and charge distributions are also determined by the code. Various electronic configurations of ^{234}U (the only isotope for which an isomer shift was measured) were simulated using the code NEWREL in order to obtain the corresponding values of $|\psi(0)|^2$. These values are shown in Table II for seven oxidation states of ^{234}U. The electrons were removed in the order of their free atom binding energies. The ordering has been found to remain constant during the process of removing the electrons one by one. The electron charge density at the center of the nucleus is represented by $|\psi(0)|^2$, at the "equivalent" nuclear radius by $|\psi(R)|^2$, and averaged over the nucleus by $|\psi_{av}|^2$. Relative changes in these three probability densities are shown graphically in Figure 4. In calculations of the change in nuclear radius, $|\psi_{av}|^2$ values have been used.

III. DISPERSION EFFECTS

When resonant Mössbauer radiation interacts with atoms, there is a possibility of interference between two inelastic processes: nuclear absorption followed by internal conversion and the photoelectric effect. Since the interaction of gamma rays with atomic electrons has predominantly electric dipole character, one expects large interference effects in the absorption spectra of Mössbauer transitions of E1 multipolarity.[24] It has been established that for E1 transitions the dispersion parameter ξ is given by:[12]

Table II

Relativistic Values of the Electron Probability Density at the Nucleus for ^{234}U

Oxidation State	Configuration (in addition to radon core)	$\|\psi(0)\|^2$ (10^7 au[a])	$\|\psi(R)\|^2$ (10^7 au[a])	$\|\psi_{av}\|^2$ (10^7 au[a])	R[b] (10^{-13}cm)
(0)	$7s^2 6d^1 5f^3$	7.88930	6.59558	6.97821	6.7675
(I)	$7s^2 6d^0 5f^3$	7.88944	6.59569	6.97834	"
(II)	$7s^1 6d^0 5f^3$	7.88923	6.59552	6.97815	"
(III)	$7s^0 6d^0 5f^3$	7.88897	6.59530	6.97792	"
(IV)	$7s^0 6d^0 5f^2$	7.88919	6.59548	6.97811	"
(V)	$7s^0 6d^0 5f^1$	7.88944	6.59569	6.97834	"
(VI)	$7s^0 6d^0 5f^0$	7.88972	6.59593	6.97859	"

[a] One au is equal to $0.538 \times 10^{+24}$ cm^{-3}.

[b] R is the "equivalent" radius of a uniformly charged nucleus.

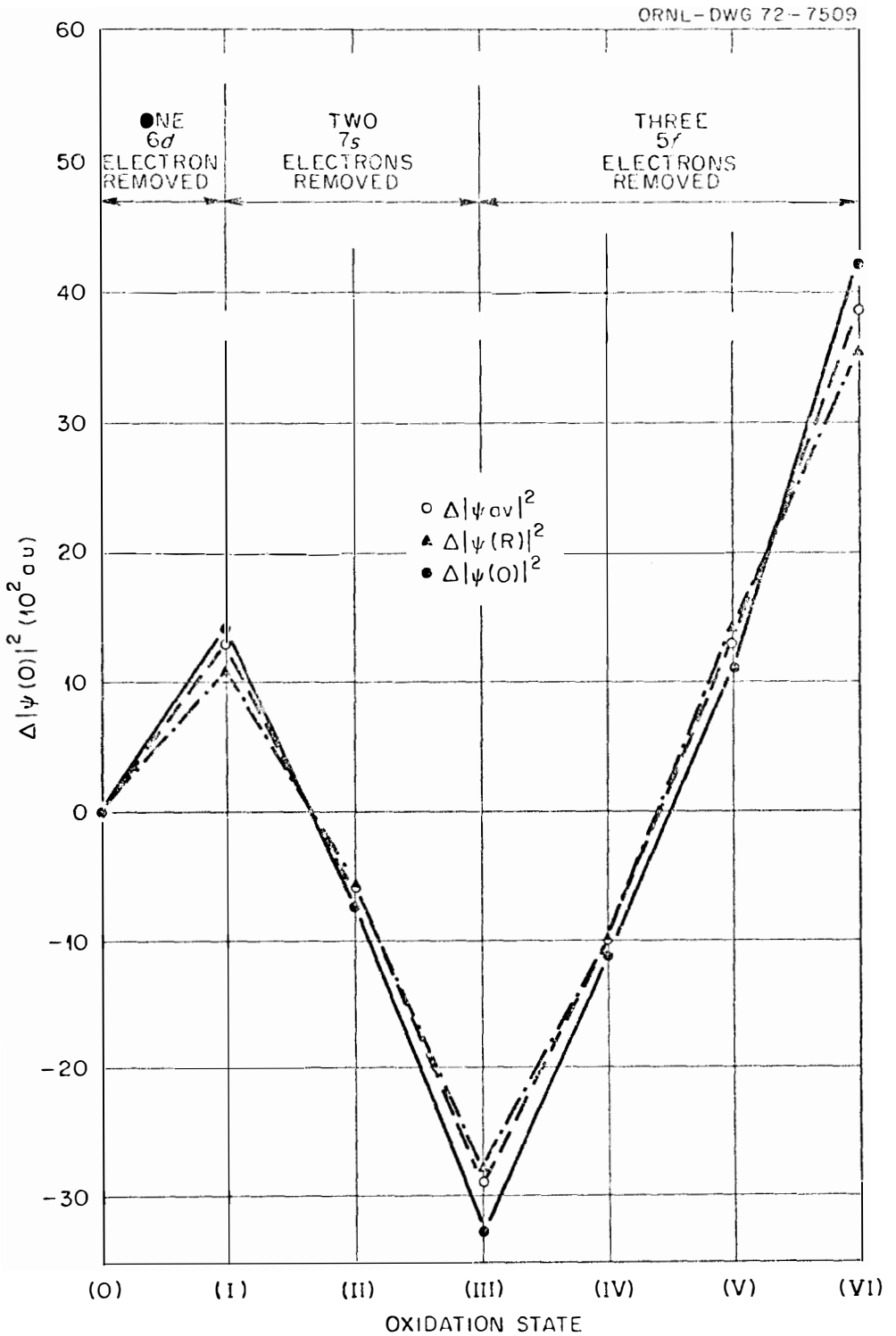

Figure 4. Changes in the relativistic electron probability density at the nucleus with the oxidation states of ^{234}U. One au is equal to $0.538 \times 10^{+24}$ cm^{-3}.

$$\xi = \varepsilon(\alpha\sigma_e' /6\pi\lambda)^{\frac{1}{2}} \tag{34}$$

where α is the internal conversion coefficient, λ is the wavelength of the incident gamma ray, σ_e' is the partial cross section for E1 photoelectric absorption, and ε is a real number which has an absolute value somewhat less than one. The quantity ε differs from one because the internal conversion coefficient and the partial cross section for photoelectric absorption are each the sum of squares of amplitudes for excitation of the atom to various final states; however, ξ is proportional to the sum of the product of these amplitudes.[25] The dominant contributions to the dispersion parameter are expected to come from the inner electronic shells, and ξ can take on either positive or negative values.[26]

The experimental amplitude of the interference or dispersion term can be obtained from a least-squares fit of the theoretical expression[27]

$$N(v) = N(\infty)\,\frac{[1 - S(1 - 2\xi X)]}{1 + X^2} \tag{34}$$

to the absorption spectrum for a single line and a thin absorber (Lorentzian approximation). Here, N(v) is the intensity transmitted at a Doppler velocity v, S is the depth of the absorption dip at resonance, ξ is the relative magnitude of the dispersion term, and $X = 2(v - \delta_{IS})/W$ or the deviation of the incident gamma ray from the resonance value in units of the half-width, W/2.

It has recently been shown that the dispersion term may also be present in the absorption spectra of gamma rays with E2 or mixed E2/M1 character.[27,28] The Mössbauer spectrum of ^{236}U for a PuO_2 source and a

UO_2 absorber was found to have a dispersion parameter, ξ, of 0.0025 ± 0.0075.[27] The investigators explain the essentially zero value of the dispersion asymmetry by the fact that the 45 keV transition in ^{236}U falls below the K electron absorption edge in uranium.[27] Values for E2 transitions in other even-even nuclei ranged from $\xi = 0.012$ to $\xi = 0.021$.[27]

The experimental isomer shifts $\delta_{IS}(\xi)$ resulting from least-squares fits of the line shape of Equation (34) are found to be different from the values $\delta_{IS}(0)$ obtained by fitting a purely Lorentzian line. For small ξ:

$$\delta_{IS}(\xi) - \delta_{IS}(0) = \kappa\xi W \tag{35}$$

where κ is a proportionality factor experimentally found to be between 1.0 and 1.2 for E2 transitions in even-even nuclei.[27] For transitions between two rotational states, the isomer shifts are normally small. Thus, the assumption of Lorentzian line shapes may lead to apparent shifts between the source and absorber which are comparable to the small isomer shifts observed.

Line broadenings due to small quadrupole interactions in the source (which are not resolved in the Mössbauer absorption spectra) may lead to an enhancement of the asymmetry effect if the quadrupole interaction is not symmetric about zero velocity (as would be the case for a $2^+ \rightarrow 0^+$ transition). In measurements of the relative isomer shifts between different absorbers, the apparent shifts due to the dispersion effect should cancel if the absorbers are thin or have the same effective thickness. A cancellation of the dispersion effect is also expected for relative isomer shifts measured with the same absorber and different sources.

CHAPTER III

EXPERIMENTAL DETAILS

I. HEALTH AND SAFETY MEASURES

In general, actinide research involves materials which are intrinsically radioactive and chemically toxic. In the course of this work, over two grams each of plutonium and uranium isotopes have been handled. These materials and their decay products emit alpha particles, beta particles, gamma rays, and also undergo spontaneous fission (see Table III for permissible body burdens and concentrations in air). For reasons of health and safety, the uranium Mössbauer experiments reported in this dissertation were conducted at the Transuranium Research Laboratory (TRL) at the Oak Ridge National Laboratory (ORNL).

The TRL is a laboratory building specifically designed with special containment features for conducting experiments with the highly toxic isotopes of the transuranium elements.[29] The unique feature of TRL operation is the practice of maintaining a "cold" or virtually contamination-free condition in all laboratories. Highly contaminated materials are confined to glove boxes and/or hoods. This permits the use of personal street clothing and avoids the requirement for items such as shoe covers and other special protective clothing. The rewards of such a system are an extra degree of freedom for the researcher in the laboratory; however, a greater degree of control at the source of potential contamination problems becomes necessary.

Table III

Permissible Doses for Internal Radiation

Isotope[a]		Critical Organ[b]	Maximum Permissible Body Burden (μg)	Maximum Permissible Air Concentration[c] (μg/cm^3)	Curies per μgram
^{234}U	(sol.)	LLI		3.2×10^{-5}	6.19×10^{-9}
		Bone	8.1	9.7×10^{-8}	
	(insol.)	Lung		1.6×10^{-8}	
		LLI		3.2×10^{-5}	
^{236}U	(sol.)	LLI		3.2×10^{-3}	6.34×10^{-11}
		Bone	$9.0 \times 10^{+2}$	9.5×10^{-6}	
	(insol.)	Lung		1.6×10^{-6}	
		LLI		3.2×10^{-3}	
^{238}U	(sol.)	LLI		6.0×10^{-1}	3.33×10^{-13}
		Kidney	$1.5 \times 10^{+4}$	2.1×10^{-4}	
	(insol.)	Lung		3.0×10^{-4}	
		LLI		6.0×10^{-1}	
^{238}Pu	(sol.)	Bone	2.3×10^{-3}	1.1×10^{-13}	1.75×10^{-5}
	(insol.)	Lung		1.7×10^{-12}	
		LLI		5.7×10^{-9}	
^{240}Pu	(sol.)	Bone	1.7×10^{-1}	8.8×10^{-12}	2.27×10^{-7}
	(insol.)	Lung		1.8×10^{-10}	
		LLI		8.8×10^{-7}	
^{242}Pu	(sol.)	Bone	$1.3 \times 10^{+1}$	5.1×10^{-10}	3.90×10^{-9}
	(insol.)	Lung		1.0×10^{-8}	
		LLI		5.1×10^{-5}	

[a]Soluble compounds of the isotope are denoted (sol.) and insoluble compounds of the isotope are denoted (insol.).

[b]The abbreviation LLI refers to the lower large intestine.

[c]Maximum permissible concentrations in air are given for a 40 hour week, occupational exposure.

Building containment features of the TRL, shown schematically in Figure 5, include: a 0.35 in. H_2O negative pressure in the entire building operating areas with respect to atmospheric pressure and a controlled negative condition in each laboratory with respect to the corridors by a fixed volume of air supply and exhaust, thus preventing the back flow of possible contaminated air to other areas of the building. The air exchange rate for each laboratory is about one laboratory volume every three minutes. Air exhausted through the laboratory and fume hood system passes first through an 80% efficient filter bank and then through a second filter bank with an efficiency of 99.95% for 0.3 micron diameter particles. All exhaust air is continuously sampled and monitored for radioactivity.

Each Mössbauer experiment dealt with approximately 1/2 g of plutonium (as a source) and 1/2 g of uranium (as an absorber). All sources, in powder form, were doubly encapsulated in aluminum cans. The absorbers, also powdered, were embedded in lucite to form compact discs of 1 3/8 in. diameter. Since both sources and absorbers were to be immersed directly in liquid helium, the single off-gas tube from the liquid helium Dewar was placed under the exhaust system normally used with a fume hood. In this way all gaseous and particulate material escaping from the Dewar could be filtered and continuously monitored as shown in Figure 5. If an accident were to occur, such as the source container rupturing, the air monitor would go off immediately. Most of the contamination would be caught in the flexible tubing of the exhaust system and the absolute filters, and any material which did escape out into the laboratory would be contained by the pressure differential.

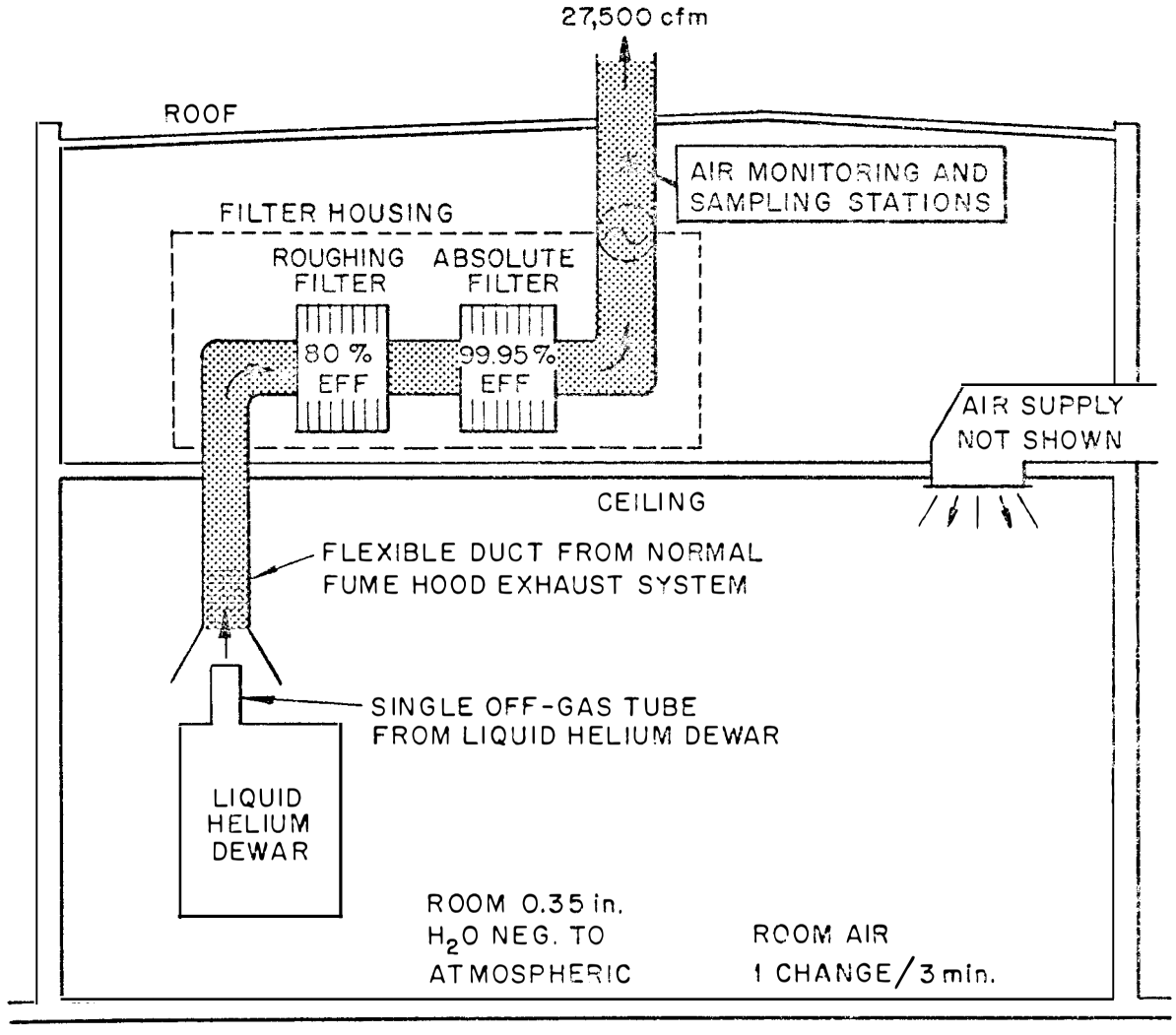

Figure 5. Safety features of the Transuranium Research Laboratory.

II. SOURCE PREPARATION

The plutonium sources used in these experiments were increasingly dangerous as the progression was made from ^{242}Pu to ^{240}Pu to ^{238}Pu. Therefore, a technique was designed and tested for ^{242}Pu which could be used for all three isotopes. Two difficulties had to be surmounted. First, the gamma rays of interest are in the 45 keV energy range and a beam of such gamma rays is readily attenuated by high density matter. In order to obtain adequate intensity, the plutonium had to be deposited in a thin (3 mil) layer over a large (1 sq in.) area to reduce the self-absorption in the source. Typically about 1/2 g of plutonium was used giving sources with a thickness of about 90 mg/cm^2 as shown in Table IV. The container walls also had to be thin (10 mils for aluminum) in order to be relatively transparent to the 45 keV gamma rays. Second, the $^{238}PuO_2$ source in particular is an extremely hazardous material; therefore, the source container had to be helium leak-tight. Otherwise, liquid helium could enter the container through small cracks and upon evaporation enlarge them and expel plutonium when the capsule was warmed to room temperature. To meet these requirements, an aluminum container was devised to doubly encapsulate the plutonium. The inner and outer containers each had 10 mil aluminum windows. A 30 mil beryllium shim was placed between the inner and outer containers for protection as shown in Figure 6.

The first set of measurements was made using readily available PuO_2 as the source of the Mössbauer gamma rays. These sources were prepared at the Thorium Uranium Recycle Facility (TURF) and the Transuranium Processing Plant (TRU) at ORNL. Isotopic purities of the source materials,

Table IV

Physical Properties of Plutonium Sources

Source	Isotopic Assay (Isotope) (%)		Heat Generation (watts/g)	PuO_2 Thickness (mg/cm^2)[a]	$PuAl_4$ Thickness (mg/cm^2)[a]
^{242}Pu	^{238}Pu	0.0004	0.00012	204.87	
	^{239}Pu	0.0015			
	^{240}Pu	0.0060			
	^{241}Pu	0.0018			
	^{242}Pu	99.99			
^{240}Pu	^{238}Pu	0.002	0.00702	87.70	
	^{239}Pu	0.762			
	^{240}Pu	98.30			
	^{241}Pu	0.764			
	^{242}Pu	0.171			
^{238}Pu	^{238}Pu	79.53	0.555	87.70	69.76
	^{239}Pu	17.06			
	^{240}Pu	2.97			
	^{241}Pu	0.333			
	^{242}Pu	0.108			

[a]Area of inner source can is 5.70 cm^2. All thicknesses reported are with respect to plutonium as a particular isotope.

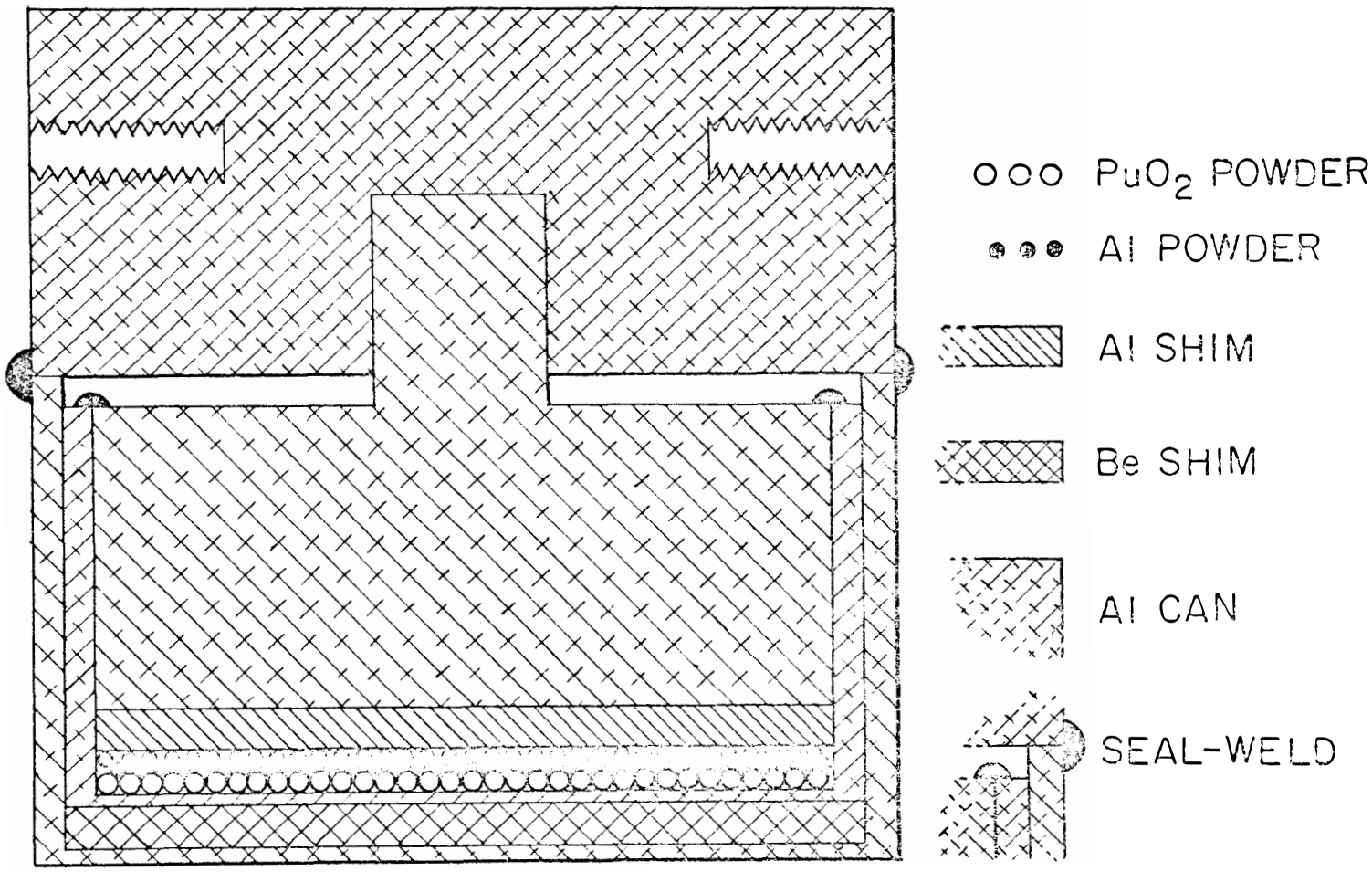

Figure 6. Schematic of the source container.

which were the best available from the Atomic Energy Commission (AEC) at that time, and the amounts of $^{242}PuO_2$, $^{240}PuO_2$, and $^{238}PuO_2$ encapsulated are shown in Table IV. After being placed in a heavily shielded radiation containment cell (hereafter referred to as cell), the PuO_2 was loaded into the inner container followed by pure aluminum powder. Both materials were spread out into a nearly uniform layer by rotating a close-fitting, thin, aluminum disc inside the can. The disc was backed by a large Teflon plunger which was carefully removed, leaving the aluminum disc in the container. An aluminum cover was pressed in to the desired depth for making the inner container seal-weld. The press fit locked the PuO_2 powder into place and prevented it from moving around.

The inner container, thus assembled, was placed in the welding turntable where a copper chill block was used to dissipate heat. The welding parameters were preset making the weld fully automatic. For the case of ^{242}Pu and ^{240}Pu, it was possible to remove the inner container from the cell after welding and decontaminate it. Leak-checks showed no obvious leaks in the seal-weld; however, an x-ray scan showed it to be rather porous. Therefore, special low temperature epoxy was placed over the weld area as an additional seal. The outer container was assembled and welded outside the cell, resulting in an excellent quality, helium leak-tight weld. A schematic of the completely assembled source container is shown in Figure 6. For the ^{238}Pu case, it was necessary to complete both the inner and outer welds inside the cell.

After the experiments had been completed with the PuO_2 sources, it was suggested that $PuAl_4$ should have a large recoilless fraction and give a narrower linewidth than the PuO_2 sources.[30] Accordingly, a $^{238}PuAl_4$ source was prepared to increase the experimental accuracy and to provide

an additional chemical state for measurements of the isomer shift in ^{234}U. The ^{238}Pu metal immediately available was from the same batch and thus of the same isotopic purity as that of the $^{238}PuO_2$ source. The alloy was prepared by levitation melting[31] and was then crushed into powder form. It was encapsulated in the same manner as the PuO_2 sources by the Isotopes Division at ORNL.

III. ABSORBER PREPARATION

As an absorber material, the non-magnetic compound $(UO_2)Rb(NO_3)_3$ was chosen since it was known to have a large electric field gradient at the uranium site.[32] The uranium isotopes (^{238}U, ^{236}U, and ^{234}U) were available in high isotopic purities from the AEC as shown in Table V, but only in the form of U_3O_8. These materials were not as hazardous as the plutonium sources; therefore, it was possible to perform all chemistry and mounting in a hood and cold lab, respectively. To prepare the compound uranyl rubidium nitrate, U_3O_8 was dissolved in concentrated nitric acid near 95°C followed by a stoichiometric amount of $RbNO_3$. The solution was evaporated overnight under a heat lamp to yield the anhydrous crystalline form. The material must be kept in a vacuum dessicator if it is to be stored for a long period of time as it tends to deteriorate in moist air.

The uranyl rubidium nitrate was transferred to TRU for mounting. The compound was ground to a fine powder in a hood using a mortar and pestle. It was then mixed with twice its own weight of Transoptic Powder (finely ground lucite available from Buehler Ltd., Evanston, Illinois). The mixture was transferred to a hardened steel die with a 1 3/8 in. inside diameter. The die was placed in an oven, heated to 200°C, removed to a press, and kept at 1000 psi while it cooled.

Table V

Physical Properties of Uranium Absorbers

Number	Absorber[a]	Isotopic Assay (Isotope) (%)		Surface Coloration[b]	Thickness (mg/cm^2)[c]
1	^{238}U	^{233}U	0.0002	yellow-green	69.77
		^{234}U	0.0008		
		^{235}U	0.0715		
		^{236}U	0.0002		
		^{238}U	99.927		
2	^{236}U	^{233}U	0.082	orange	61.94
		^{234}U	0.0017		
		^{235}U	0.205		
		^{236}U	99.68		
		^{238}U	0.034		
3	^{234}U	^{233}U		brown spots in yellow-green	34.65
		^{234}U	86.61		
		^{235}U	8.965		
		^{236}U	0.168		
		^{238}U	4.257		
4	^{234}U	^{233}U	0.020	yellow	41.24
		^{234}U	94.78		
		^{235}U	0.091		
		^{236}U	0.046		
		^{238}U	5.06		

[a]The compound $(UO_2)Rb(NO_3)_3$ was used for all four absorbers.

[b]The colors reported other than yellow-green were from surface layers only and did not affect the Mössbauer resonance.

[c]Area of absorber is 9.57 cm^2. All thicknesses reported are with respect to uranium as a particular isotope.

Absorber thicknesses are listed in Table V. Ideally the plastic discs were yellow-green in color (the intrinsic color of uranyl rubidium nitrate). However, if the die became too hot, a yellow or orange surface layer formed on the sample due to the decomposition of the uranyl rubidium nitrate to oxides of rubidium (yellow) and UO_3 (yellow-orange). This was only a surface effect and did not alter the quality of the Mössbauer resonance. Four samples were prepared in all: one each of ^{238}U and ^{236}U, and two of ^{234}U. A second ^{234}U absorber was fabricated because the first contained iron or chromium impurities (brown). Since better isotopic purities were available by the time the $PuAl_4$ source was packaged, it was decided to obtain additional material for the final experiments.

IV. MÖSSBAUER SPECTROMETER

With the exception of those even-odd nuclei with very low-lying excited states, most Mössbauer sources and absorbers must be cooled to liquid nitrogen or liquid helium temperatures to produce any appreciable recoilless emission or absorption of gamma rays. This is especially true for the 45 keV resonance in uranium. The one run taken at liquid nitrogen temperature with the $PuAl_4$ source showed no apparent effect. Thus all results reported in this work were done at liquid helium temperatures.

A metal Dewar with a main liquid hemium cavity and smaller liquid nitrogen cavity (as shown schematically in Figure 7) was used. The inner liquid helium Dewar was fabricated from stainless steel and held 35 liters. Loss rates were encountered of about one liter per hour. Both the source container and the absorber disc were in direct contact with the liquid helium. The absorber was connected to the velocity drive by a 36 in. hollow stainless steel rod. The drive motor remained out of the

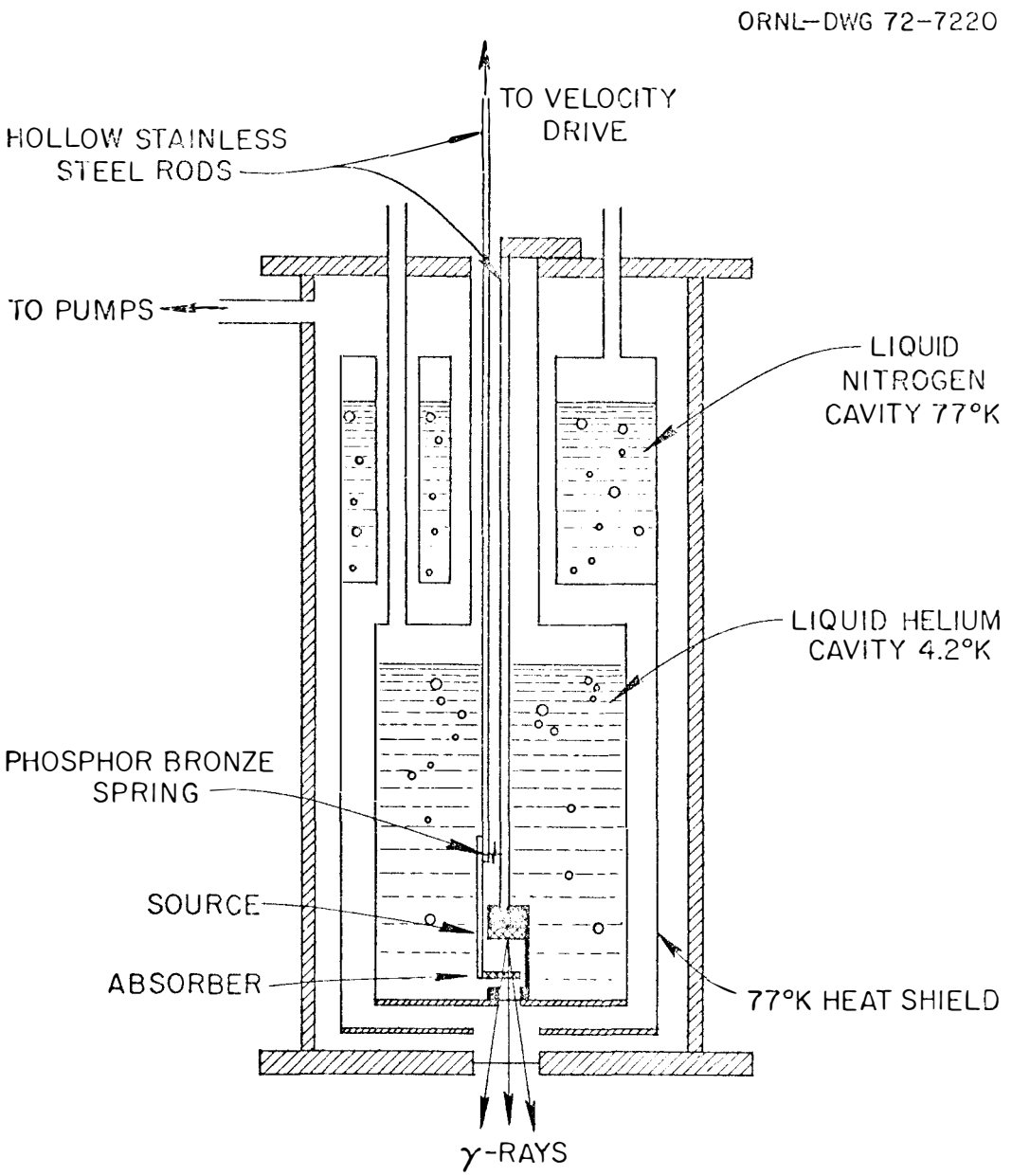

Figure 7. Schematic of the cryostat.

liquid helium, at approximately room temperature, and in all experiments the absorber was moved with respect to the source. The beryllium window at the bottom of the helium can was 1 1/4 in. in diameter and 80 mils thick.

The liquid nitrogen can was made of copper and held 15 liters. The liquid helium Dewar was screened from room temperature radiation by a copper heat shield attached to the liquid nitrogen container. When no liquid helium was present the vacuum jacket could be pumped down to a pressure of 10^{-6} torr, and when the liquid helium was added, the pressure dropped to 10^{-8} torr. The beryllium window at the bottom of the outermost can was 2 in. in diameter and 20 mils thick. The entire metal Dewar assembly weighed about 600 pounds and was mounted on a concrete-block structure by means of rubber pads intended to dampen out any extraneous room vibrations.

The gamma rays for the 45 keV resonance in uranium were detected by a 7 cm^2 surface area x 0.4 cm depletion depth Nuclear Diodes Ge(Li) detector with a resolution of 2.3 keV at 60 keV. The plutonium source was positioned at a distance of 7 in. from the detector. The detector was powered by a regulated dc high voltage supply operated at 600 volts. After passing through a Nuclear Diodes preamplifier, the gamma ray pulses were amplified by a Tennelec TC 203BLR amplifier and base line restorer. A TC 440 single channel analyzer was gated on the gamma ray of interest. The gamma rays for the 14.4 keV resonance in iron were detected by a Reuter-Stokes gas-filled proportional counter operated at 1875 volts. The signals were amplified by a DD2 amplifier followed by a single channel analyzer set on the 14.4 keV gamma ray.

Basically the Mössbauer spectrometer has two functions: to provide a relative velocity between the source and absorber in a controlled, reproducible manner and to correlate the detected resonance gamma rays with the instantaneous velocity. A block diagram of the initial electronic configuration is shown in Figure 8. The first requirement is fulfilled by a sine-wave electromechanical transducer driven with a negative feedback system, and the second with a multichannel analyzer (MCA) operating in the multiscaler mode and synchronized with the transducer velocity. This MCA stores the detector pulses selected by the single channel analyzer.

The transducer consisted of an armature rigidly attached to a drive coil which oscillated inside a cylindrical Alnico magnet. Attached to the top of the armature was a bar magnet which oscillated inside an extremely accurate high-velocity pickup coil[33] (see Appendix A). This armature was connected to a rigid mounting block via three phosphor-bronze springs. The attachment method permitted free movement along a vertical axis. The transducer was sinusoidally driven near its resonance frequency by a Krohn-Hite model 4025(R) oscillator operating through the external reference input of a Mössbauer drive unit developed by Dr. J.O. Thomson.[34] The pickup coil was designed to be linear and insensitive to sidewise motion of the transducer to one part in 10^5 (for vertical motions of less than one millimeter in amplitude). The vertical motion of the armature induced an AC voltage in the pickup coil which was proportional to the velocity. This particular drive assembly is capable of attaining velocities of up to ±300 mm/sec.

Two separate multichannel analyzer configurations were employed. The initial configuration will be designated (i) and the revised

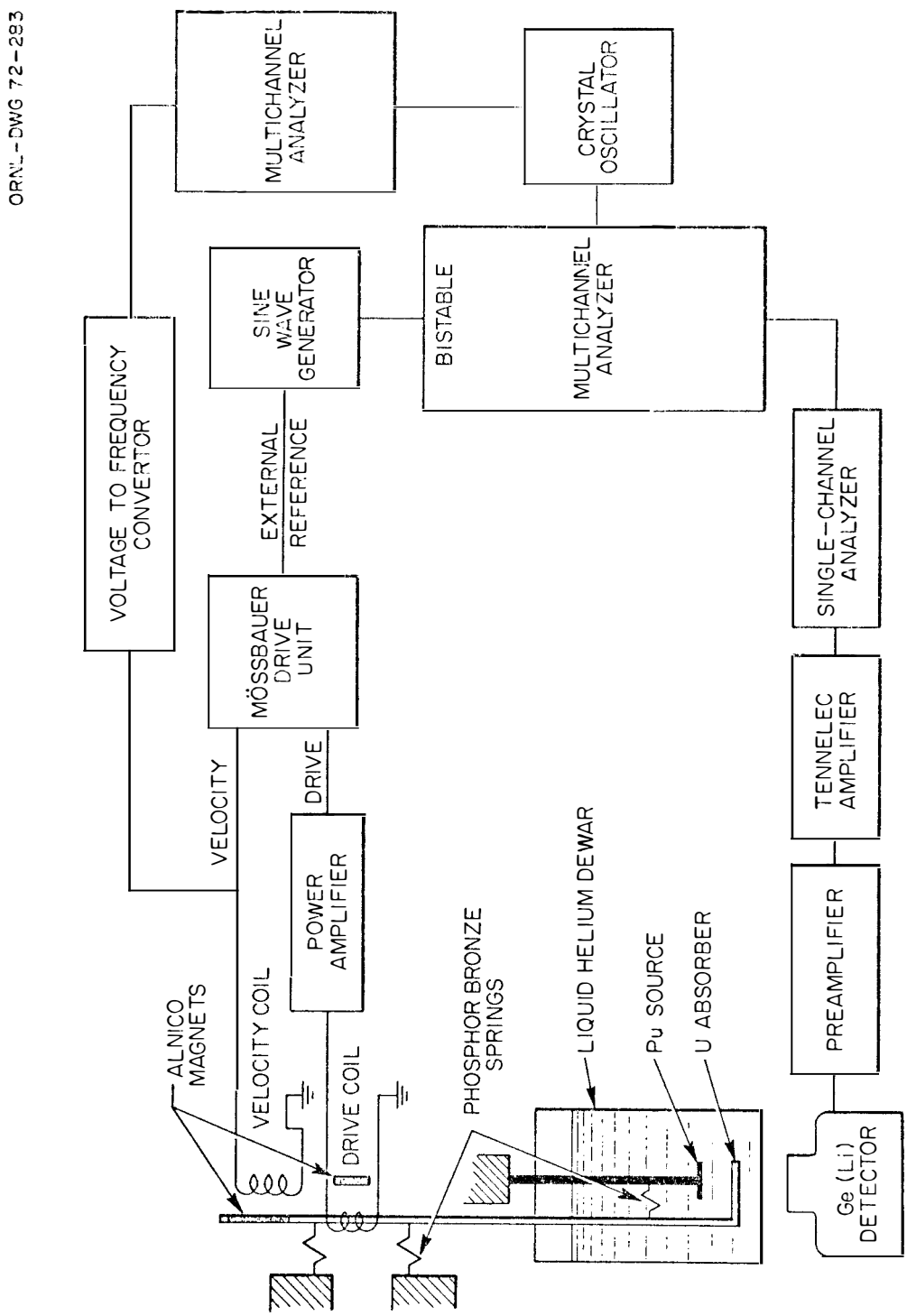

Figure 8. Block diagram of the initial electronic configuration.

configuration will be designated (r). For the initial configuration shown in Figure 8, a 400 channel RIDL analyzer and a 200 channel RIDL analyzer were stepped in parallel by means of a crystal oscillator (see Figure 9) also designed by Dr. J.O. Thomson. Briefly, the main (front) output of the crystal oscillator was used to sequentially step the channels of the 400 channel RIDL operating in the time mode. The bistable of the 400 channel RIDL was then connected to the SYNC input of the Krohn-Hite 4025(R) oscillator set at a frequency just above the resonance frequency of the transducer. The frequency of the crystal oscillator and the vernier frequency control of the Krohn-Hite 4025(R) were then adjusted so that the Krohn-Hite quadrature sine-wave output and the bistable of the 400 channel RIDL were synchronized in frequency and phase. The rear output of the crystal oscillator was designed to operate at exactly 1/2 the frequency of the main (front) output. This symmetric square wave was used to step the 200 channel RIDL through 200 channels in the same time that the 400 channel RIDL was stepped through 400 channels by the main output.

These two multichannel analyzers provided the option of taking two spectra simultaneously. The uranium Mössbauer spectrum was stored in the 400 channel RIDL. The 200 channel RIDL collected counts from a voltage to frequency convertor (Krohn-Hite 5400 Signal Generator) which had been connected to the AC voltage output of the pickup coil. Thus a "spectrum" of the velocity waveform could be obtained simultaneously with that of the uranium Mössbauer spectrum. Experimental details of the PuO_2(i) Mössbauer runs are shown in Table VI.

For the $^{238}PuAl_4$ source, the major objective was to obtain an accurate determination of the isomer shift and the dispersion parameter.

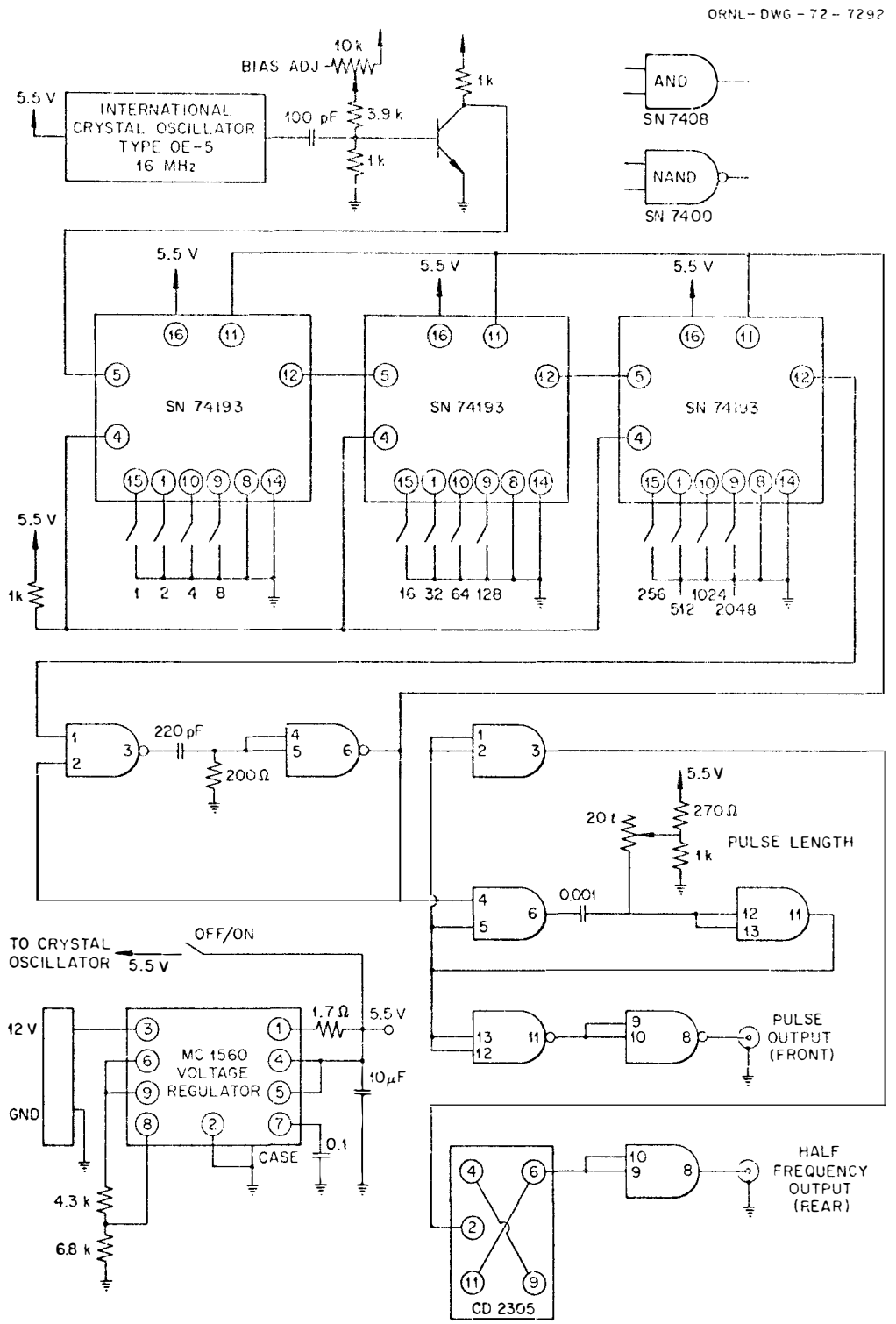

Figure 9. Circuit diagram of the crystal oscillator.

Table VI

Experimental Details of Mössbauer Runs

Source	Absorber Number[a]	Run Time (hrs)	Number of Channels	Background Cts/Channel	Velocity (mm/sec)	Drive Frequency (cps)
$^{242}PuO_2$(i)	1	299.36	400	14,580	182.5	12.9
$^{240}PuO_2$(i)	2	93.35	400	575,800	142.7	12.9
$^{238}PuO_2$(i)	3	38.06	400	2,532,000	142.7	12.9
$^{238}PuAl_4$(r)	4	54.00	1024	2,123,000	142.7	15.3
$^{238}PuO_2$(r)	4	53.29	1024	2,339,000	142.7	16.6

[a]The compound $(UO_2)Rb(NO_3)_3$ was used for all four absorbers.

To provide greater flexibility and more channels, a 2200 series analyzer from Nuclear Data Incorporated was used. This 4096 channel analyzer could be operated in the dual multiscaler mode with approximately zero dead time. Again the Krohn-Hite 4025(R) was synchronized with the bistable of the Nuclear Data analyzer and the crystal oscillator was used to step the channels. A block diagram of the revised experimental configuration is shown in Figure 10.

Only 2048 channels were used at a time. The uranium spectrum was collected in the first bank of 1024 channels and a one-line iron spectrum with the source mounted at the top of the armature was simultaneously collected in the second bank of 1024 channels. Whenever it was necessary to fill with liquid helium, the analyzer was stopped. After the fill, a short calibration run was taken. The spectrum of the velocity waveform was collected in the third bank of 1024 channels simultaneously with a one-line iron spectrum in the fourth bank of 1024 channels. Then the analyzer was allowed to continue accumulating counts in the uranium/iron banks.

In this manner an overall iron calibration (second bank of 1024 channels) was obtained for determining the time-averaged zero velocity. The series of iron spectra accumulated in the fourth bank of 1024 channels showed whether or not zero velocity had drifted during the run. The velocity waveform was analyzed to determine its harmonic content (even harmonics shift the position of zero velocity). To compare accurately the isomer shifts and dispersion parameters of the $^{238}PuAl_4$ source and $^{238}PuO_2$ source, it was necessary to run the $^{238}PuO_2$ source again with the revised experimental configuration and the new ^{234}U absorber. Experimental details of these runs are shown in Table VI.

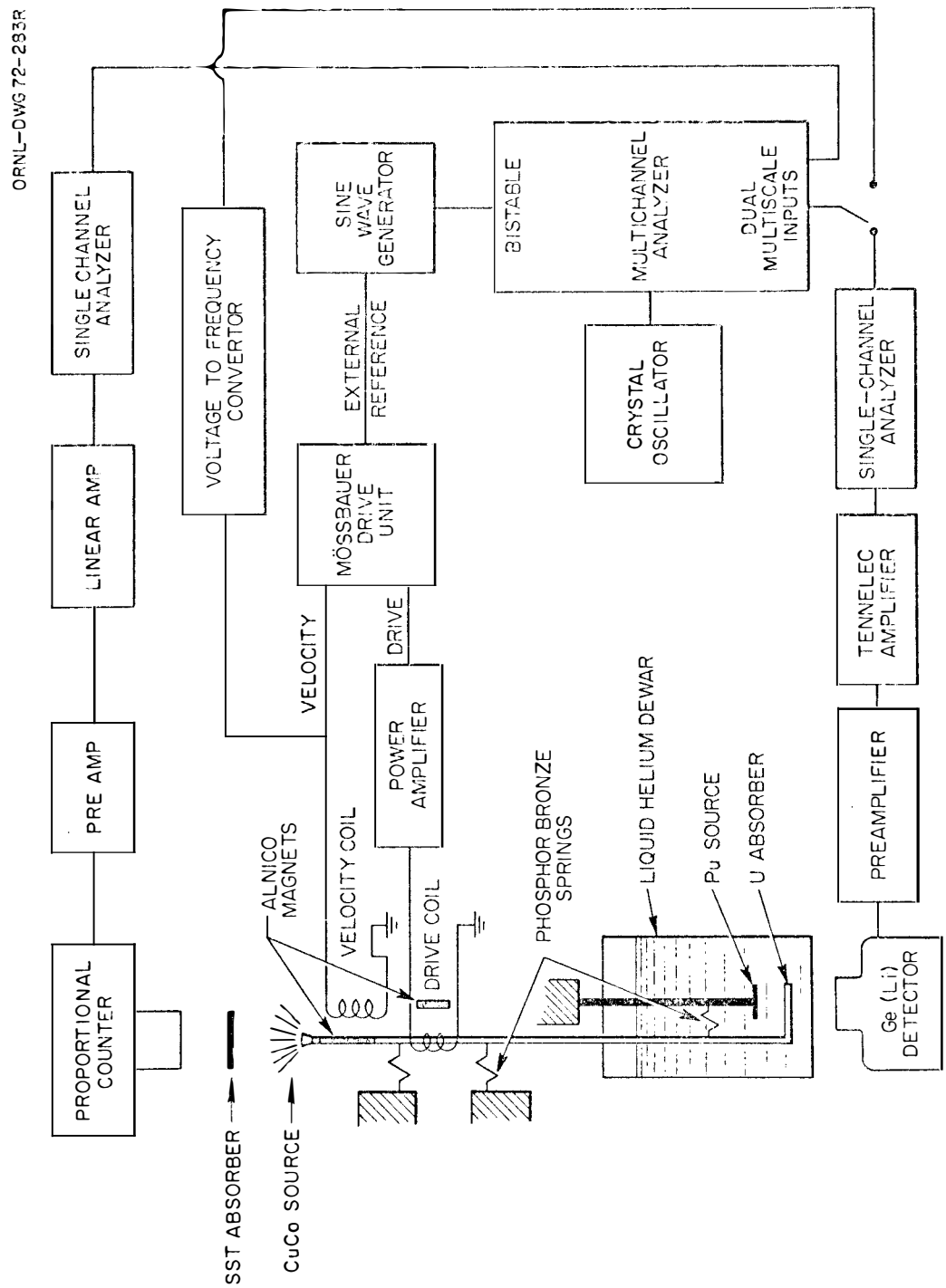

Figure 10. Block diagram of the revised electronic configuration.

V. CALIBRATION

In all cases, the maximum velocity was determined in the same manner. The high-velocity pickup coil was initially calibrated using a six-line iron spectrum. A Cu(Co) source was mounted at the top of the armature and run versus an Armco iron absorber (1/2 mil foil) at various velocities ranging from 20 mm/sec to 185 mm/sec. At low velocities, the difference in velocity units of the outermost iron lines(10.657 mm/sec)[35] was used to calculate the maximum velocity of the sine-wave. The velocity scale for higher velocity ranges was determined by the ratio of the rms voltage readings.

The velocity waveforms were analyzed by a fast Fourier transform (FFT) computer code written by M.R. Patterson (see Appendix B). The Fourier coefficients were determined up to and including the Nyquist frequency, forcing the computed curve to pass through all of the data points. Thus the harmonic content of the waveform was obtained. Since several short calibrations were taken during a run, it was possible to check the stability of the sine-wave velocity. In treating the data, the velocity waveform was put into the least-squares fitting program along with the uranium Mössbauer spectrum so that a point-by-point determination of the velocity corresponding to each channel could be obtained (see Appendix C).

For the runs with the Nuclear Data analyzer, the maximum velocity and the calibration spectra were treated in the same manner as the runs with the RIDL analyzers. In addition, to make sure that the zero velocity was correctly determined, the one-line iron spectra [Cu(CO) source versus a 1 1/2 mil stainless steel absorber] which were run at the same velocities as the uranium spectra were analyzed. The channel number

position of the iron line corrected for the isomer shift of -0.37 mm/sec[36] determined the channel number position of zero velocity for a source moving at the top of the armature. This channel number was compared to the channel number corresponding to the zero velocity of the calibration spectrum. In all cases they were offset by a constant amount thought to be dependent on a phase lag between the armature motion and the voltage to frequency convertor output.

An additional check on the transducer was made by simultaneously running two Cu(Co) versus stainless steel Mössbauer spectra, one at the top of the armature and one at the bottom of the armature, in the dual multiscaler mode (1024 channels each) at a velocity of 142.7 mm/sec. Corrections could thus be made for the fact that the sine-wave velocity of the top of the armature did not faithfully reproduce that of the bottom of the armature.

VI. DATA ANALYSIS

A computer least-squares fitting routine named LSFMTI (Least-Squares Fit to a Mössbauer Transmission Integral)[37] and developed by Dr. John Burton was used to analyze the Mössbauer absorption spectra measured in these experiments. In order to compute the theoretically expected absorption spectrum, the energy distribution of the emitted gamma rays must be multiplied by the fraction of gamma rays which will be transmitted through the absorber, and this product integrated over all energies. The resulting expression is called the transmission integral. To analyze a Mössbauer spectrum, a least-squares fit to the data must be obtained for the transmission integral by appropriate choice of the various parameters.

The computer code fits the data with a curve of the form

$$AC(E_s) = AO\left[(1 - CB) + \frac{CB \cdot 2}{\pi W_s} \int_{-\infty}^{\infty} \frac{dE\ e^{-\sum_{j=1}^{n} \frac{S_j}{\left(\frac{E - E_j}{W_j/2}\right)^2 + 1}}}{\left(\frac{E - E_s}{W_s/2}\right)^2 + 1}\right] \qquad (36)$$

where $AC(E_s)$ is the computed intensity at the energy E_s; AO is a normalization factor; S_j, E_j, and W_j are the intensity, position, and full width at half-maximum for the jth absorption line; n is the number of absorption lines; W_s is the natural width of the source; and CB is the recoilless fraction of the source, including background corrections. The integral in Equation (36) cannot be evaluated in closed form. However, the first two terms of a power series expansion of the exponential in the integrand lead to integrals which can be evaluated analytically. The remaining terms are calculated by a 48-degree Gauss-Legendre quadrature.[38]

With a given set of parameters W_s, S_j, E_j, and W_j the integral portion of Equation (36) is evaluated. By standard least-squares fitting, the best fit of the linear parameters, AO and CB, is then determined. Next, the value of χ^2 is computed. Variations in the parameters are performed until a minimum value of χ^2 is reached (within the prescribed accuracy for the parameters).

Instead of working with all the possible parameters for a least-squares fit, various constraints may be imposed. The values of W_s, CB, S_j, E_j, or W_j may be either fixed or free independent parameters, or they may be computed as a linear function of some other independent parameters. In the analysis of the uranium spectra, the widths W_j were made equal to one independent variable; the E_j were determined from the isomer shift

and the quadrupole splitting parameter (effectively constraining the position of the unresolved line); and the S_j were made proportional (2:2:1) to one total effective thickness parameter. To investigate interference effects, the dispersion term was added to the transmission integral. In Equation (36), S_j was multiplied by the expression: $1 - 2\xi \frac{(E - E_j)}{W_j/2}$, and ξ was included as an independent parameter in the least-squares fitting procedures.

An error analysis is part of the program and is used to compute the statistical errors for the independent and dependent parameters. All errors quoted in this work are one standard deviation as computed by the code unless otherwise noted. Plotting of the data, error bars, and the fitted curve is performed on a Calcomp plotter. A curve corresponding to each component of a multiple line spectrum is also plotted and the curves are smoothed between data points by a third order interpolation.

Since the absorbers are driven both toward and away from the source, a mirror image of the spectrum is obtained in the second-half of the channels used for each run. Program LSFMTI is written to fit both sets of data. Each half is therefore labelled first-half or second-half. The program then folds the second-half onto the first-half about a channel which makes the isomer shift of the first-half equal to the isomer shift of the second-half. The summed spectrum is then refit, replotted, and labelled folded. It is the folded spectra which are shown in this work. The folding routine eliminates to first order the sinusoidal background caused by the sinusoidally driven, radioactive absorber.

CHAPTER IV

EXPERIMENTAL RESULTS AND DISCUSSION

I. SOLID STATE PROPERTIES OF SOURCES AND ABSORBERS

The compound uranyl rubidium nitrate was used as an absorber for all the Mössbauer experiments reported here. The crystal is a member of the hexagonal system (rhombohedral division). The primitive rhombohedron has lattice parameters $a = 8.30 \pm 0.03$ Å and $\alpha = 68°42' \pm 20'$ and contains two stoichiometric molecules.[39] The corresponding six-molecule hexagonal unit has $a = 9.36 \pm 0.03$ Å and $c = 18.88 \pm 0.06$ Å.[39] The x-ray intensity data of Hoard and Stroupe show conclusively that both uranium and rubidium lie on body-centered rhombohedral lattices and that the origins of the two lattices are separated by exactly c/4 along the unique axis as shown by the atomic arrangement of Figure 11.[39] The linear uranyl groups all lie parallel to the c axis of the crystal, each surrounded by three nitrate groups in the equatorial plane. The U-O distance in the $(UO_2)^{++}$ ion was estimated by Hoard and Stroupe to be 1.58 Å; Zachariasen[40] has suggested a value of 1.63 Å, based on an empirical correlation of bond length and bond strength in $(XO_2)^{++}$ ions. Recent Raman and infrared spectroscopic studies[41] confirm that the uranyl ion is linear, and the latest x-ray studies[42] find the uranium-oxygen bond length in the uranyl ion to be 1.78 Å. In any case, this is very much smaller than the distance of 2.72 Å between the uranium atom and its next nearest neighbors, the six oxygen atoms in the nitrate groups. The nitrates are thought to have little effect on the strong uranyl bonding. A schematic of the

ORNL DWG 72-284A

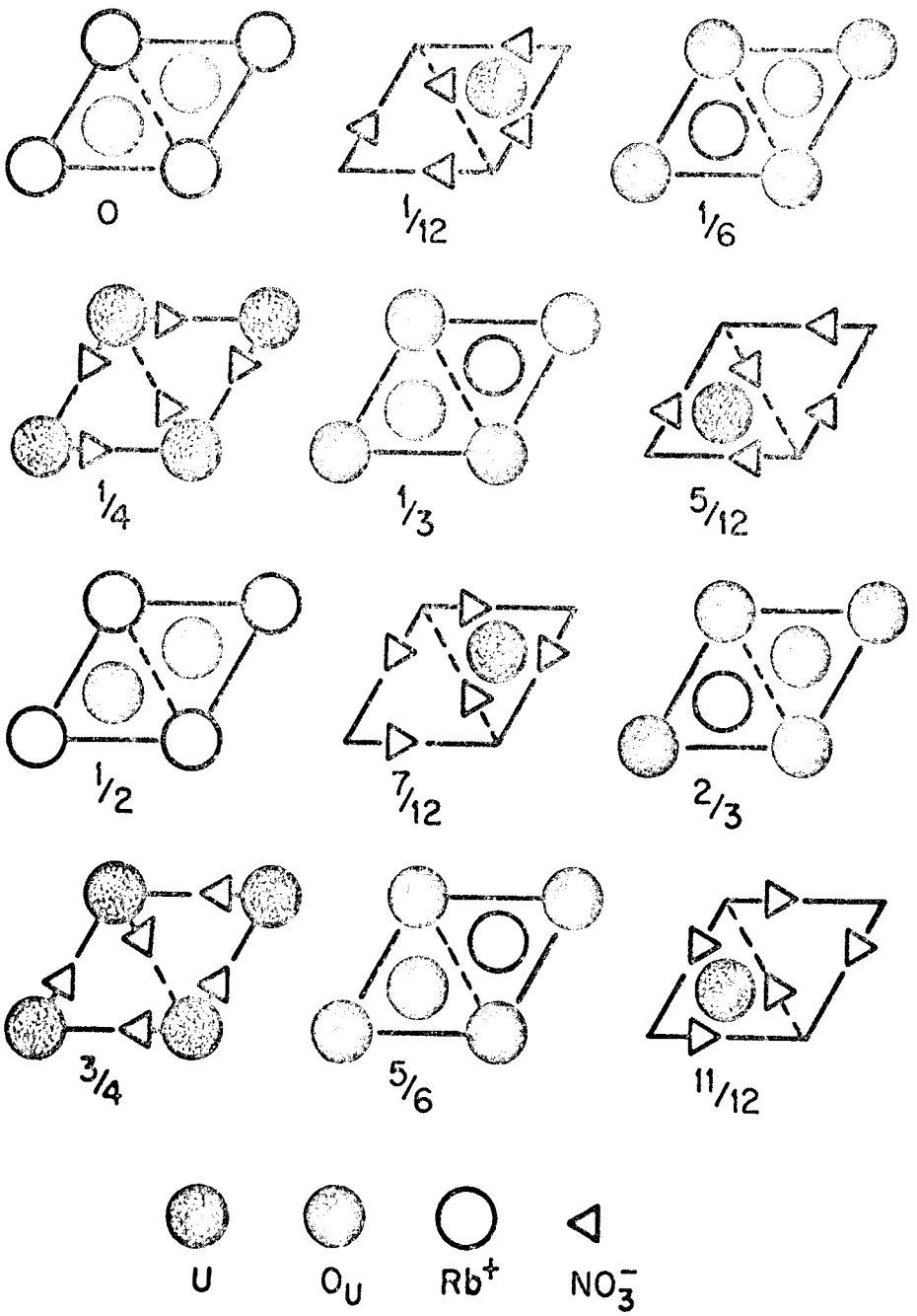

Figure 11. Atomic arrangement in uranyl rubidium nitrate. The atoms are drawn approximately to scale; the numbers are displacements along the crystalline c axis, expressed as fractions of the lattice period.

molecule is shown in Figure 12. Due to the high degree of symmetry of the molecule, the η term of the quadrupole interaction (see Chapter II) has been neglected in the data analysis.

The first three Mössbauer experiments were made with PuO_2 sources using three different plutonium isotopes (^{242}Pu, ^{240}Pu, and ^{238}Pu). The compounds PuO_2 and UO_2 both exhibit the face-centered cubic fluorite (CaF_2) structure.[43] There are four plutonium and eight oxygen atoms per unit cell. The oxygen atoms are in simple cubic packing within the unit cell which is bounded by plutonium atoms at the cell corners and face-centered positions as shown in Figure 13. The room temperature lattice constant of PuO_2[44] is 5.3960 ± 0.0003 Å which is similar to that of UO_2 (5.4700 ± 0.0001 Å[44]). The interatomic distance between the plutonium atom and its eight oxygen nearest neighbors is 2.336 Å.

The plutonium dioxide structure possesses cubic symmetry at the plutonium site (which rules out a quadrupole interaction), is non-magnetic,[13] and therefore should produce a single line source. However, it has been reported by Rand, Fox, and Street[45] that the lattice parameters of plutonium compounds increase continuously with time when kept sealed at room temperature. It is suggested that this increase is due to the displacement of atoms to interstitial sites by the recoil of alpha emission. For PuO_2 the relative change in the lattice parameter may be represented by an exponential growth equation of the form[46]

$$\Delta a/a = 3.38 \times 10^{-3}[1 - \exp(-\beta t/\tau)], \qquad (37)$$

where β is a constant equal to 1.23×10^4 for PuO_2 and τ is the lifetime

ORNL DWG 72-282A

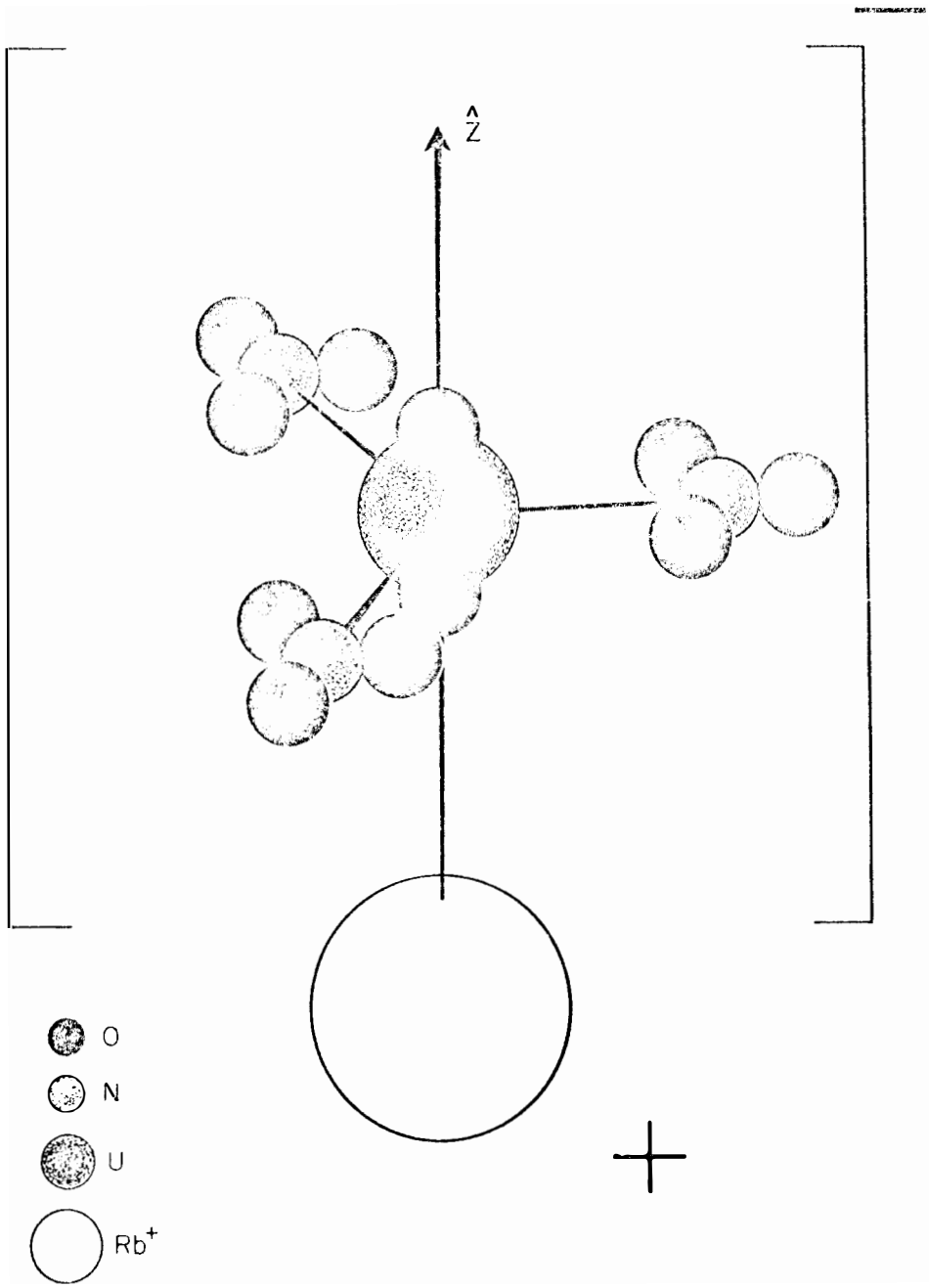

Figure 12. Structure of the uranyl rubidium nitrate molecule. The three nitrate groups are shown lying in a plane perpendicular to the collinear O-U-O entity.

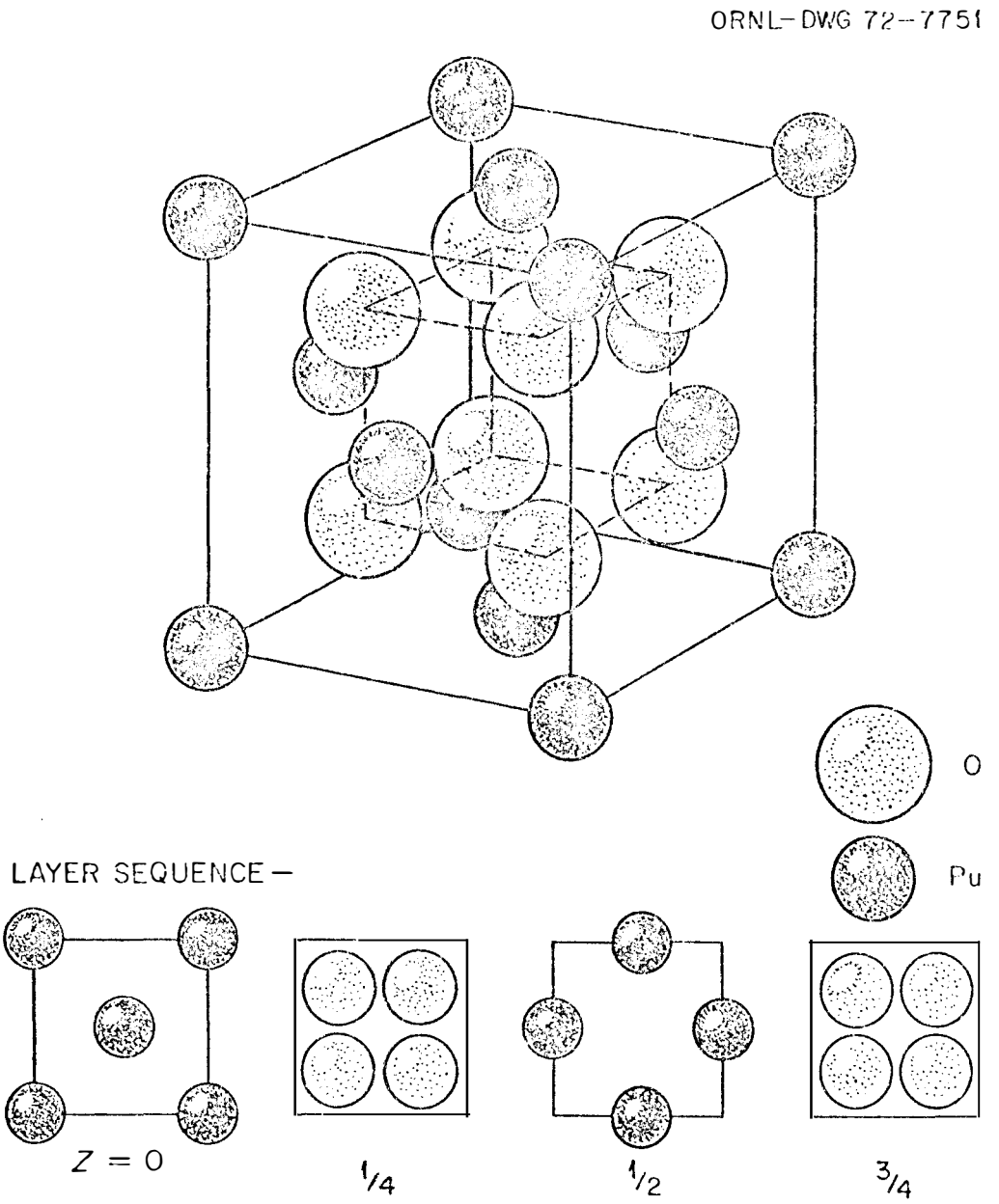

Figure 13. The fluorite structure formed by PuO_2.

of the plutonium isotope. For ^{238}Pu the exponential time constant (τ/β) is 3.68 days. It has been estimated that about 1500 Frenkel defects (vacancies in which an atom is transferred to an interstitial position) are produced per alpha disintegration,[47] so that the saturation concentration of Frenkel defects is between one-half and one defect pair (vacancy and interstitial) per unit cell. The x-ray data indicate that no inhomogeneous strain is introduced by the self-irradiation damage.[45]

The Frenkel defects in the PuO_2 structure may give rise to small electric field gradients since the plutonium site no longer possesses cubic symmetry. Small quadrupole interactions in the source which are not resolved in the Mössbauer spectra could produce asymmetric broadenings of the absorption lines. The broadening will be asymmetric because the quadrupole interaction for a 2^+ excited state and an 0^+ ground state is not symmetric about zero velocity (see Chapter II). Such unresolved quadrupole interactions lead to an apparent dispersion effect as mentioned in Chapter II.

In order to obtain information from another source with differing electronic structure and a narrower line width, a Mössbauer spectrum was taken with a $PuAl_4$ source. This intermetallic compound exhibits the body-centered orthorhombic UAl_4 structure[48] and has four formula units per unit cell. The lattice constants are similar to those of UAl_4:

UAl_4[48]	$PuAl_4$[49]
a = 4.41 ± 0.02 Å	4.396 ± 0.001 Å
b = 6.27 ± 0.02 Å	6.266 ± 0.001 Å
c = 13.71 ± 0.03 Å	13.708 ± 0.002 Å

and the structure of $PuAl_4$ is shown in Figure 14. The Pu-Al distance is

ORNL-DWG 72-8157

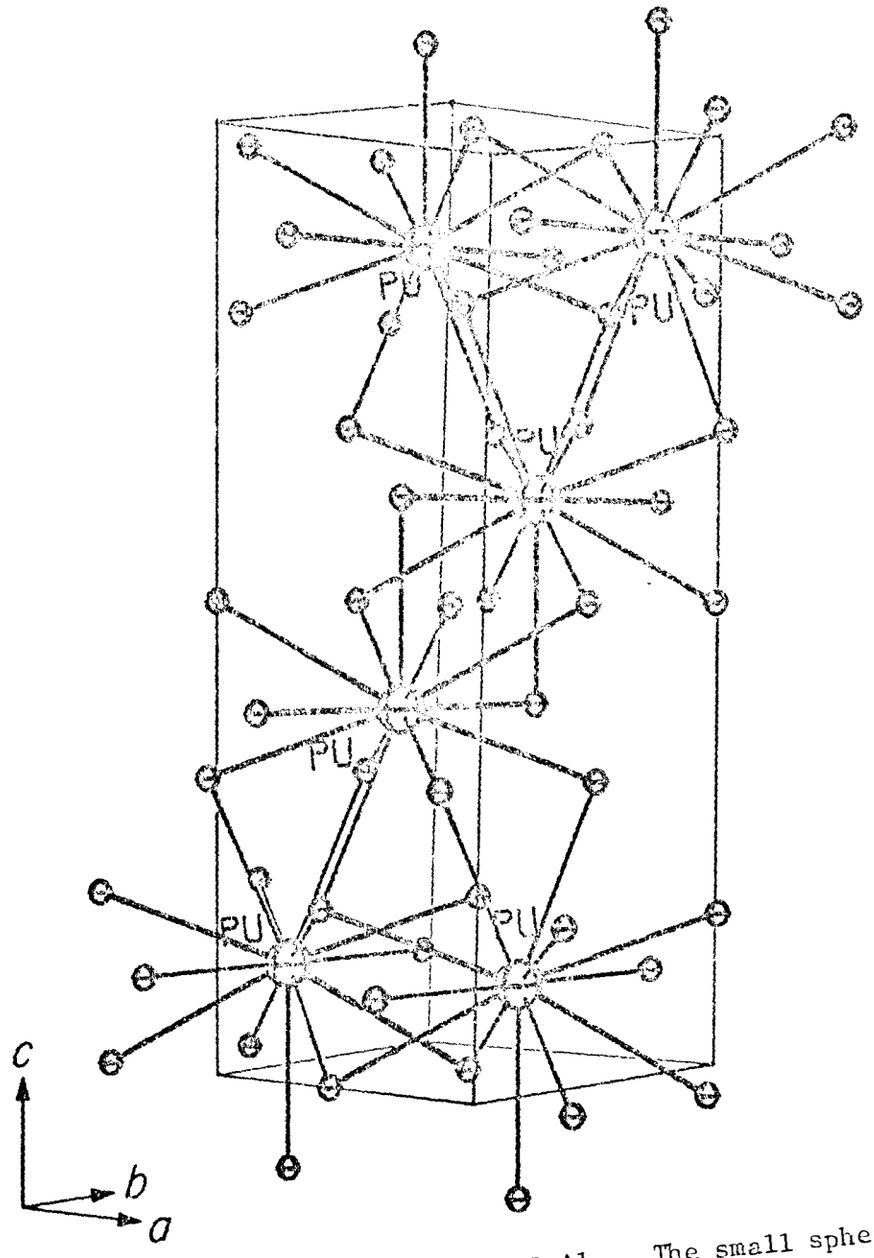

Figure 14. The structure of $PuAl_4$. The small spheres represent aluminum atoms.

the same in the c-direction as in the b-direction and is equal to 3.133 Å or half the length of the unit cell side b.

Although the plutonium site in this compound does not possess cubic symmetry, Mössbauer results in americium[30] have shown that $PuAl_4$ sources produce a narrower linewidth than PuO_2 sources. Evidence for a large vacancy concentration has been provided by both chemical analyses and density measurements and indicates that the compocition is near $Pu_{0.9}Al_4$.[49] The lattice parameters of plutonium-aluminum alloys have been found by Ellinger, Land, and Miner[50] to increase after ten years storage at room temperature. Ellinger attributes this fact to the diffusion of aluminum, but Rand[45] claims that self-irradiation damage similar to that seen in PuO_2 is more probable. Again electric field gradients at the plutonium site may result from these vacancy concentrations and Frenkel defects. However, the asymmetric line broadening should be smaller than that for the PuO_2 sources, since the self-irradiation damage effect is expected to be smaller in the intermetallic compound $PuAl_4$ than in the insulator PuO_2.

II. COMPARATIVE MÖSSBAUER RESULTS FOR ^{238}U, ^{236}U, AND ^{234}U

The folded Mössbauer spectra of ^{238}U, ^{236}U, and ^{234}U for PuO_2 sources and $(UO_2)Rb(NO_3)_3$ absorbers are shown in Figures 15, 16, and 17, respectively. The initial electronic configuration was used for these experiments. In the computer fits, the line positions have been constrained to retain the 3:1 splitting ratio and the intensities of the lines have been constrained to have the ratio 1:2:2 for the 0, ±1, and ±2 states, respectively. Dispersion terms were not included in the computer fits. The largest percent effect was obtained for ^{238}U, but the counting

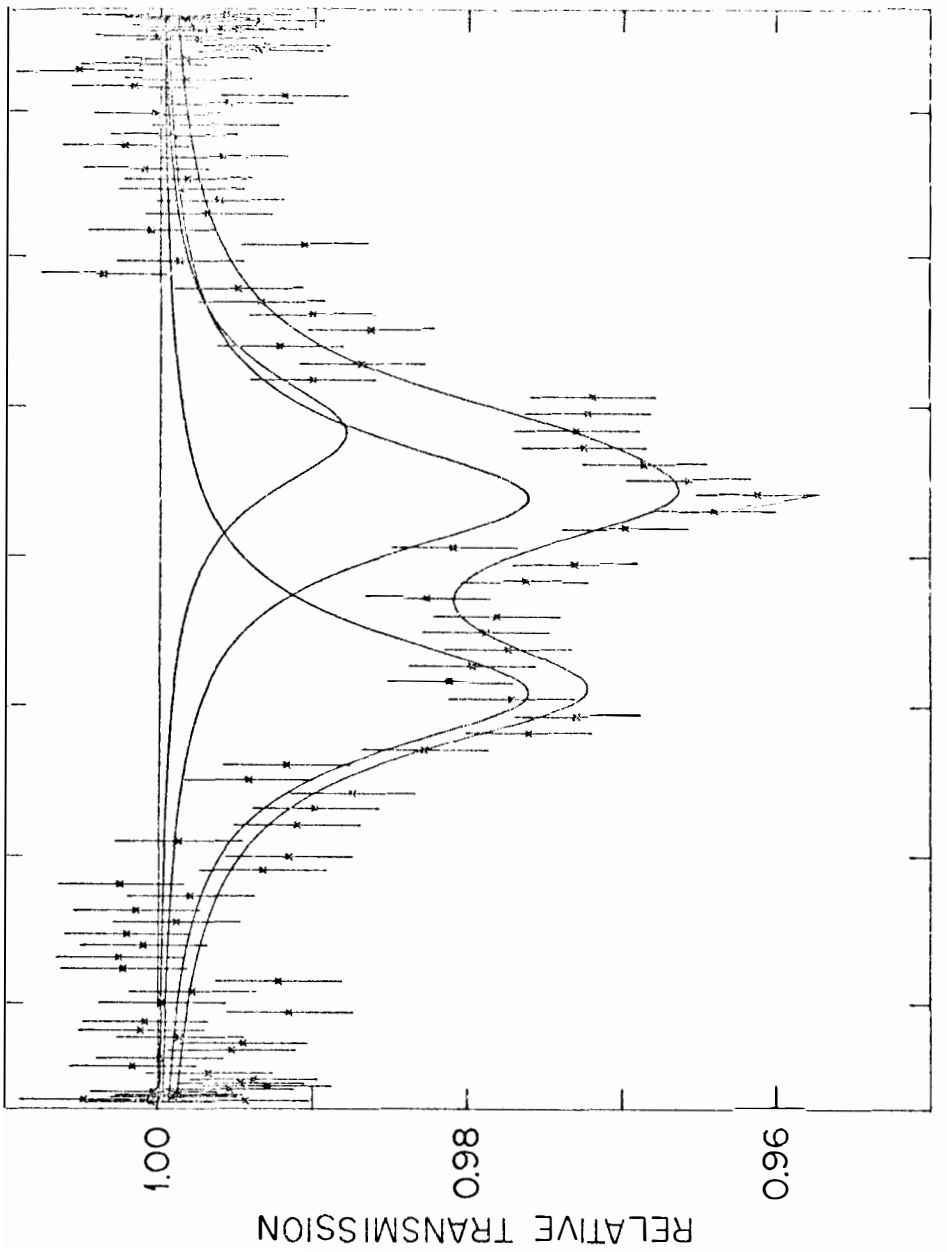

Figure 15. Mössbauer spectrum of ^{238}U in $(UO_2)Rb(NO_3)_3$ following the alpha decay of ^{242}Pu in PuO_2 at 4.2° K. The initial electronic configuration was used.

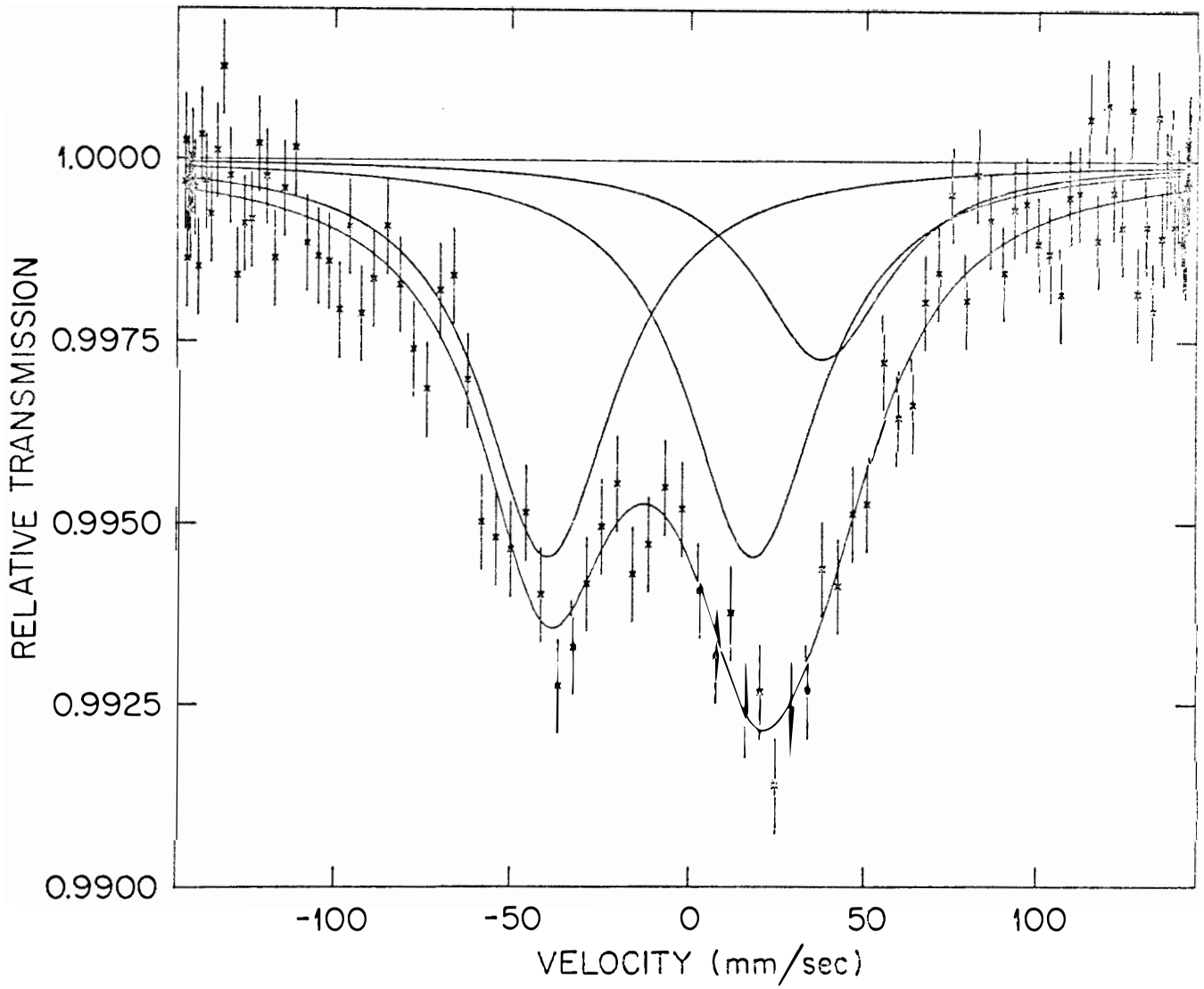

Figure 16. Mössbauer spectrum of ^{236}U in $(UO_2)Rb(NO_3)_3$ following the alpha decay of ^{240}Pu in PuO_2 at 4.2° K. The initial electronic configuration was used.

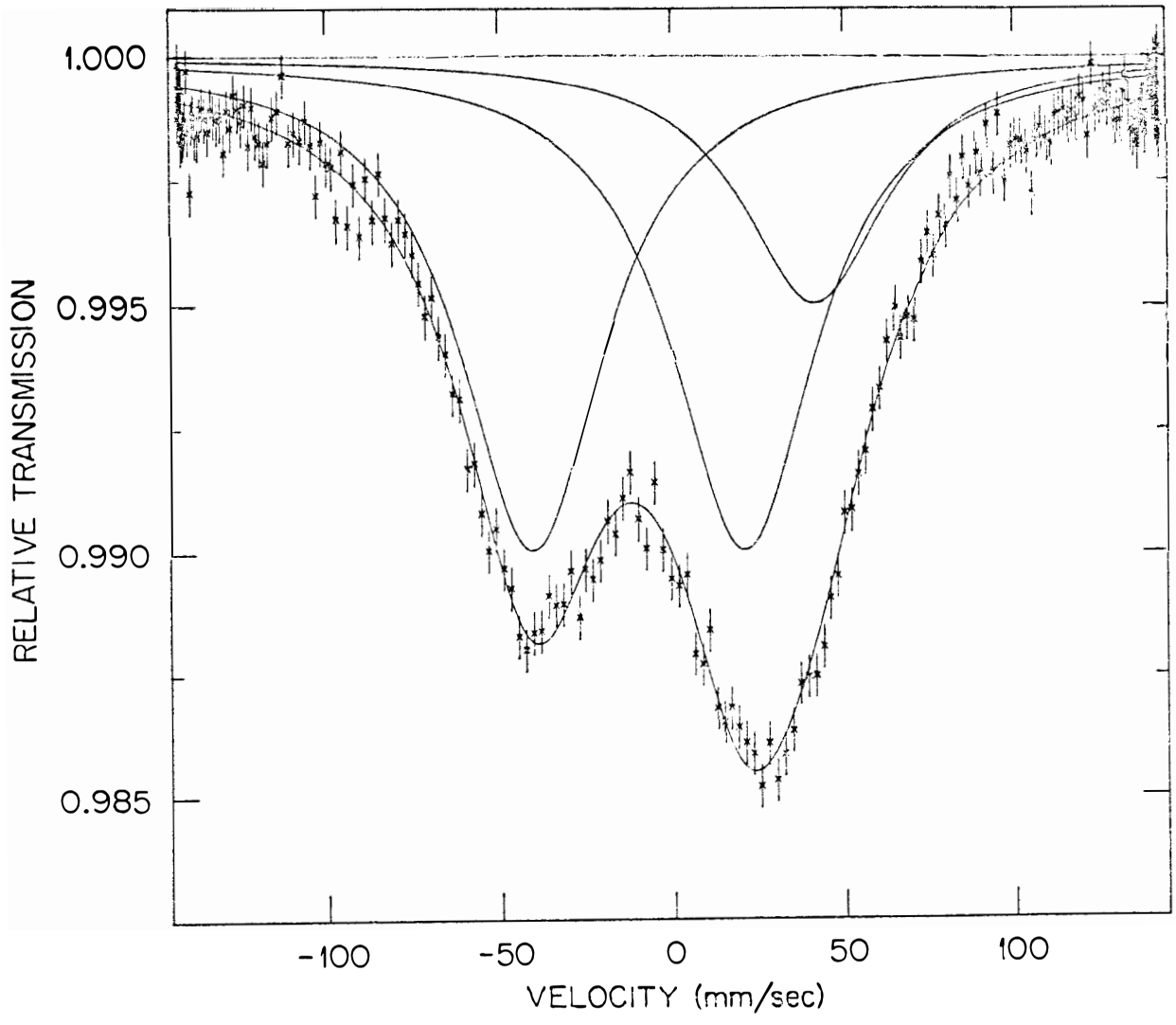

Figure 17. Mössbauer spectrum of ^{234}U in $(UO_2)Rb(NO_3)_3$ following the alpha decay of ^{238}Pu in PuO_2 at 4.2° K. The initial electronic configuration was used.

rate was the lowest for this isotope. The ^{234}U spectrum had the highest counting rate and therefore showed the most promise for further study. The solid curve in these figures is a least-squares fit of the full transmission integral to a pure quadrupole interaction in the absorber where η has been assumed to be zero [see Equation (22)]. The three component curves have been included in each plot. The parameters obtained from all three uranium spectra are collected in Table VII.

The isomer shift term of Equation (33) has not been observed within experimental errors for any of the three isotopes studied with the initial experimental configuration. The same absorber compound was used for all three runs; therefore, q, the negative of the average crystalline electric field gradient at the uranium site [see Equation (19)] has been assumed to be a constant. This leads to the following quadrupole moment ratios:

$$Q238/Q234 = 1.10 \pm 0.07$$

$$Q236/Q234 = 0.98 \pm 0.05.$$

These values agree fairly well with others recently determined by Mössbauer measurements[11] and from B(E2) values.[51] The ratios differ slightly from those previously reported by the author[8,9] due to the fact that the full transmission integral was used to fit the data reported here instead of the Lorentzian approximation which was used in the earlier analysis.

Since the spectra are asymmetric about zero velocity, both the magnitude and sign of the quadrupole coupling constant can be determined. The intrinsic quadrupole moment of the ^{234}U nucleus is known from B(E2) values[51] to be $Q_o = 10.19 \pm 0.13 \times 10^{-24}$ cm^2. The relation between the

TABLE VII

Measured Mössbauer Parameters for PuO_2 Sources Versus $(UO_2)Rb(NO_3)_3$ Absorbers[a]

Nucleus	Intensity (total for all three lines) (%)	Γ_{exp} FWHM (mm/sec)[b]	3/8 eqQ (mm/sec)[b]	δ_{IS} (mm/sec)[b]
^{234}U	2.5	50.4 ± 0.8	-61.4 ± 0.7	-0.3 ± 0.4
^{236}U	1.4	46.2 ± 2.6	-58.1 ± 2.6	-1.6 ± 1.6
^{238}U	6.1	48.6 ± 3.8	-65.4 ± 3.9	-1.8 ± 2.2

[a]The initial electronic configuration was used for these experiments.

[b]Systematic errors have been included in the data.

spectroscopic quadrupole moment and the intrinsic quadrupole moment in the strong coupling model is given by Equation (24). Since K is equal to zero for the first rotational band in even-even nuclei, one finds that $Q = -2/7\ Q_o$ or $Q = -2.91 \pm 0.04 \times 10^{-24}$ cm^2 for the ^{234}U nucleus. Using the value of 3/8 eqQ (velocity units) = -61.4 ± 0.7 mm/sec (see Table VII) as the velocity differential, one obtains a corresponding energy differential of 3/8 eqQ (energy units) = $-8.91 \pm 0.10 \times 10^{-6}$ eV [see Equation (1)], and the resulting value of q is $8.16 \pm 0.14 \times 10^{18}$ V/cm^2. This negative electric field gradient at the uranium nucleus which is directed parallel to the crystalline z axis (the O-U-O axis) is evidence that the bonding produces a concentration of electronic charge in the x-y plane in confirmation of results from previous nuclear orientation studies.[32]

Eisenstein and Pryce[13] predicted that the bonding electrons of the uranyl ion would form a column of charge along the O-U-O axis. However, Roberts and Dabbs have shown these studies to be incorrect[52] and have established that the uranyl bond is clearly covalent, that π bonding is excluded and that the quadrupole interaction must arise either from σ bonding or from bonding states dominated by $Y_{3,\pm3}$ or $Y_{2,\pm2}$. The conclusions of Eisenstein and Pryce rest on the assumption that the σ bonding dominates. Roberts and Dabbs make the point that one can only reverse their conclusion by assuming the bond to have roughly half its charge (two electrons) involved in the covalent aspect of the bond and the other two electrons in a nonbonding configuration constructed from $Y_{3,\pm3}$ or $Y_{2,\pm2}$. It is unusual in the chemistry of bonding to find such a strong covalent bond with the oxygens monovalent and with the two available electrons on an adjacent atom in a nonbonding configuration. However, the much more chemically reasonable configuration proposed by Eisenstein

and Pryce can lead to rather unexpected nuclear results (negative quadrupole moment for ^{237}Np).

For the ^{234}U spectrum, a computer fit was performed in which the line positions were unconstrained. The intensity ratios were forced to retain the values of 1:2:2 and the widths of the absorption lines were made equal to one independent variable. In this fit an optimum comparison between the data and the theoretical line shape was found to occur for a splitting ratio of (3.37 ± 0.26):1. Such an effect might be caused by a small quadrupole interaction in the source, a non-zero value for η [see Equation (17)], or the next highest term (hexadecapole) in the multipole expansion [see Equation (26)]. In order to account for the splitting ratio suggested above, a value of $emM/64 = -0.20 \pm 0.14$ mm/sec or $-2.8 \pm 2.0 \times 10^{-8}$ eV would be required. The intrinsic hexadecapole moment of the ^{234}U nucleus is thought to be[53] $M_o = 4.16 \pm 0.54 \times 10^{-48}$ cm^4 and is the largest of any nucleus yet studied. The relationship between the spectroscopic hexadecapole moment and the intrinsic hexadecapole moment is given by Equation (30). One finds that $M = 1/21\ M_o$, or $M = 1.98 \pm 0.26 \times 10^{-49}$ cm^4 for the ^{234}U nucleus. Using the above value for emM/64, one obtains a value for m of $-9.1 \pm 6.6 \times 10^{42}$ V/cm^4.

Estimates have been made for m in uranyl rubidium nitrate by assuming a linear uranyl group aligned on the z axis with the uranium atom at z = 0. A single negative charge was assigned to each oxygen atom and the uranium-oxygen distance was taken to be 1.78 Å.[42] The fourth derivative of the Coulombic potential due to these two negative charges was calculated (calc) at the uranium site and found to be $m_{calc} = 3.9 \times 10^{33}$ V/cm^4. Neither the sign nor the magnitude agrees with the experimental value given above. However, according to Sternheimer[54] the calculated value for m must be multiplied by a hexadecapole antishielding factor if it is

to agree with the experimental result. Values of the hexadecapole anti-shielding factor, $1 - \eta_\infty$, as large as 1 + 63000 have been calculated.[54] If a value of $1 + 10^6$ were assumed for this factor, the experimental value of m should be $+3.9 \times 10^{39}$ V/cm^4 which is still too small by a factor of 10^3 and of the opposite sign. Therefore, it seems unlikely that the hexadecapole interaction is causing the non 3:1 ratio of the splittings.

A non-zero value for η could also cause the splitting ratio to differ from 3:1 [see Equation (17)]. The raising and lowering operators $\hat{I}_+$ and $\hat{I}_-$ will introduce off-diagonal elements into the Hamiltonian matrix. However, the η term seems unlikely, due to the three-fold symmetry at the uranium site in the absorber compound, uranyl rubidium nitrate, and the fact that the O-U-O bonds are linear and all lie parallel to the z axis of the crystal.

There is still the possibility of a quadrupole interaction in the PuO_2 source, since one-half to one Frenkel defect per unit cell is expected to result from self-irradiation damage. The plutonium sites will no longer possess cubic symmetry and electric field gradients may occur. An estimate has been made of the magnitude of the quadrupole interaction in the source which would cause the full width of each of the absorption lines at half maximum (FWHM) to be 50.4 mm/sec when the minimum observable FWHM is only 23.3 mm/sec. The emission line, for simplicity, was assumed to be the sum of two Lorentzian lines of equal intensity and each possessing the minimum observable linewidth; the absorber line was assumed to be unsplit. The separation between these two lines was found to be about 23 mm/sec and should be a rough estimate of the average quadrupole interaction in the source. Using a value[51] of 11.25×10^{24} cm^2

for the intrinsic quadrupole moment of ^{238}Pu, the magnitude of q at the plutonium site in $^{238}PuO_2$ should be about 3 x 10^{18} V/cm^2. The quadrupole splitting for a 2^+ to 0^+ transition is expected to be asymmetric about zero velocity (see Figure 3, page 16) and thus the quadrupole interaction in the source should alter the 3:1 splitting ratio in the absorber.

A computer fit was also performed in which the intensities of the absorption lines were unconstrained. The line positions were constrained to the 3:1 splitting ratio and the widths of the absorption lines were made equal to one independent parameter. The ratio of the intensities remained 1:2:2 within the limits of experimental error.

III. COMPARATIVE MÖSSBAUER RESULTS FOR ^{234}U

The folded Mössbauer spectra of ^{234}U for $PuAl_4$ and PuO_2 sources which were taken using the revised electronic configuration are shown in Figures 18 and 19, respectively. In these data the percent effect is larger, and the linewidth has decreased over that previously found for ^{234}U in Figure 17. The fact that the percent effect is larger for the PuO_2 source run with the revised experimental configuration than that for the PuO_2 source run with the initial experimental configuration is probably due to the absence of any chemical impurities in the new absorber. In the computer fits of a theoretical lineshape to the data (shown as a solid line through the data points), the line positions have been constrained to have the splitting ratio of 3:1 and the intensities of the lines have been constrained to the ratio 1:2:2 for the 0, ±1, and ±2 states, respectively. The parameters obtained from these spectra, analyzed with and without the dispersion term, are listed in Table VIII. All isomer shifts have been corrected using the results of the Cu(Co) versus

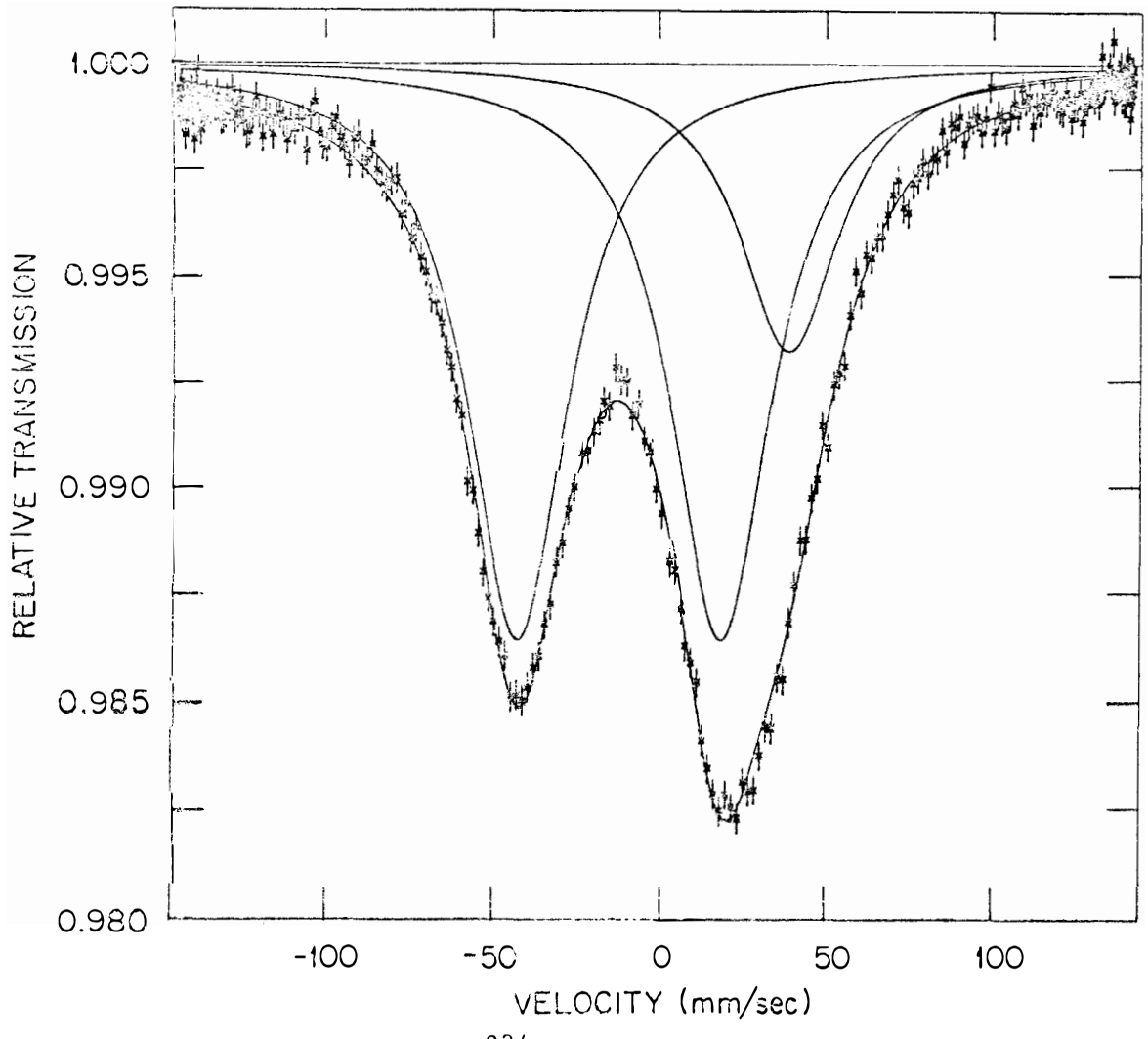

Figure 18. Mössbauer spectrum of ^{234}U in $(UO_2)Rb(NO_3)_3$ following the alpha decay of ^{238}Pu in $PuAl_4$ at 4.2° K. The revised electronic configuration was used.

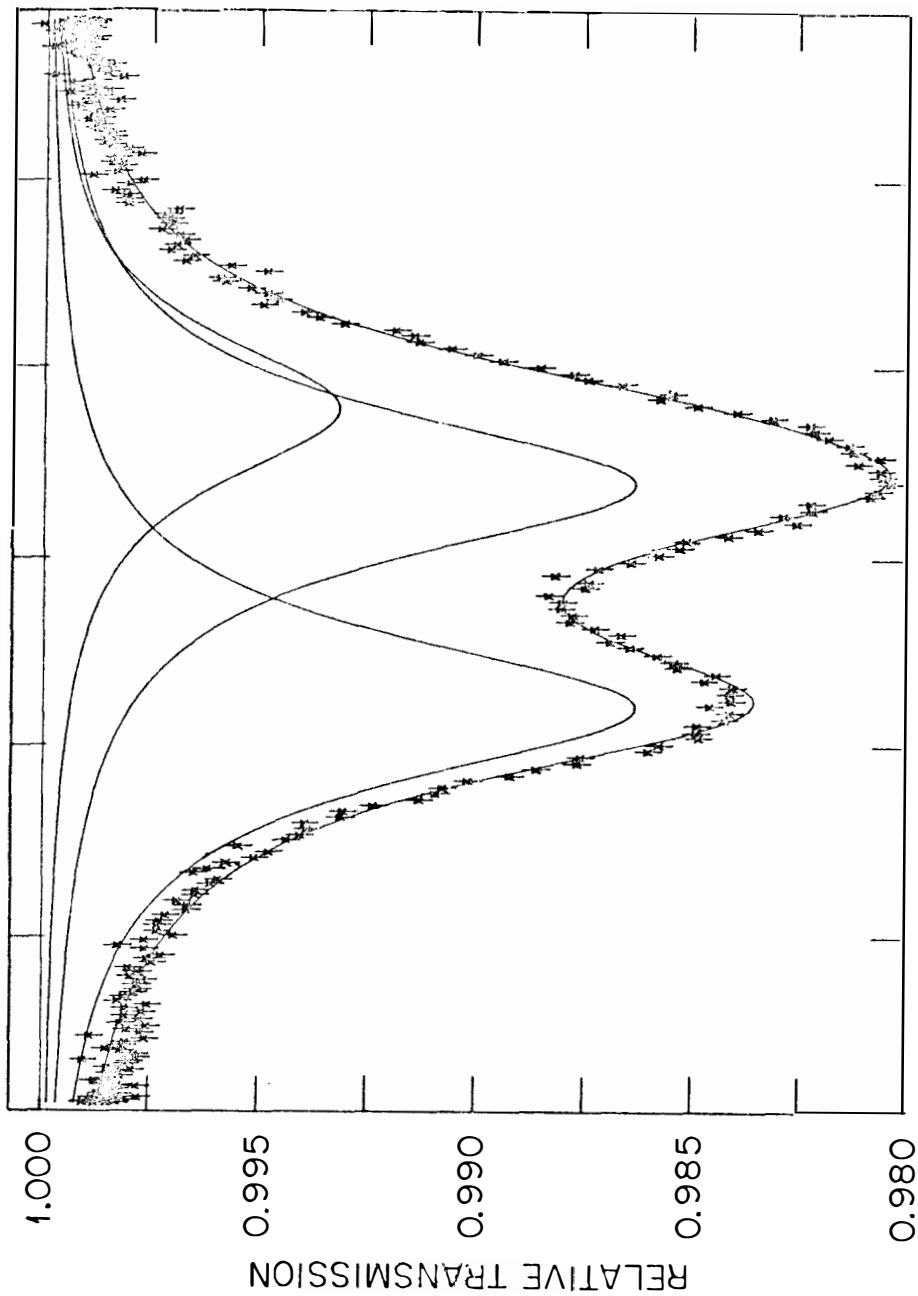

Figure 19. Mössbauer spectrum of ^{234}U in $(UO_2)Rb(NO_3)_3$ following the alpha decay of ^{238}Pu in PuO_2 at 4.2° K. The revised electronic configuration was used.

TABLE VIII

Measured Mössbauer Parameters for $^{238}PuO_2$ and $^{238}PuAl_4$ Sources Versus $(^{234}UO_2)Rb(NO_3)_3$ Absorbers[a]

Source	Intensity (total for all three lines) (%)	Γ_{exp} FWHM (mm/sec)	3/8 eqQ (mm/sec)	δ_{IS} (mm/sec)[b]	ξ
$^{238}PuO_2$	3.4	48.31 ± 0.38	-58.77 ± 0.24	-0.40 ± 0.33	0.0
$^{238}PuO_2$	3.4	47.04 ± 0.35	-58.92 ± 0.21	1.23 ± 0.35	0.025 ± 0.002
$^{238}PuAl_4$	3.4	36.51 ± 0.33	-60.45 ± 0.21	-1.27 ± 0.31	0.0
$^{238}PuAl_4$	3.4	36.53 ± 0.31	-60.57 ± 0.21	-0.69 ± 0.33	0.013 ± 0.003

[a]The revised electronic configuration was used for these experiments.

[b]Isomer shifts have been calibrated using the -0.37 mm/sec isomer shift of Cu(Co) versus stainless steel to determine zero velocity.

stainless steel Mössbauer spectra run simultaneously with the uranium spectra to determine zero velocity.

The weighted average for the quadrupole coupling constant for ^{234}U for the three runs $^{238}PuO_2$(i), $^{238}PuO_2$(r), and $^{238}PuAl_4$(r) using the same absorber compound, uranyl rubidium nitrate, is:

$$3/8\ eqQ = -59.75 \pm 0.54\ mm/sec = -8.67 \pm 0.08 \times 10^{-6}\ eV.$$

This gives a value for the negative of the electric field gradient at the uranium site of:

$$q = 7.94 \pm 0.13 \times 10^{18}\ V/cm^2.$$

The isomer shift for the $^{238}PuO_2$(r) run is -0.40 ± 0.33 mm/sec when the dispersion term is neglected and agrees with that of -0.3 ± 0.4 mm/sec for the $^{238}PuO_2$(i) run.

The isomer shift for the alloy $^{238}PuAl_4$ is -1.27 ± 0.31 mm/sec when the dispersion term is neglected. The oxidation state of Pu in PuO_2 is normally assumed to be (IV), and the oxidation state of U in $(UO_2)Rb(NO_3)_3$ is normally assumed to be (VI). Since $PuAl_4$ is an intermetallic compound, the plutonium atom in this compound cannot immediately be assigned an oxidation state. However, Pillinger and Stone[55] give a value for the isomer shift between $NpAl_4$ and $(NpO_2)Rb(NO_3)_3$ which is 1.44 times that for the isomer shift between NpO_2 and $(NpO_2)Rb(NO_3)_3$. The ratio of $\Delta|\psi_{av}|^2$ for a (III) oxidation state source and a (VI) oxidation state absorber to that for a (IV) oxidation state source and a (VI) oxidation state absorber is 1.41.[23] Therefore the isomer shift in the alloy $NpAl_4$ seems to be characteristic of an oxidation state of (III) for the Np in a non-conducting compound. For this reason, the oxidation state of

Pu in $PuAl_4$ is here assumed to be (III).

The isomer shift in $^{238}PuAl_4$ enables us to give an estimate of the change in nuclear radius between the excited and ground states in ^{234}U nuclei as shown in Equation (33). The change in electronic charge density for an absorber of oxidation state (VI) and a source of oxidation state (III) in ^{234}U is 67×10^2 au or 36.1×10^{26} cm^{-3} (see Table II, page 20). Using the value of -1.27 ± 0.31 for the isomer shift of the $^{238}PuAl_4$ source versus the uranyl rubidium nitrate absorber, one obtains a relative change in nuclear radius of:

$$\Delta R/R = -3.4 \pm 0.8 \times 10^{-6}.$$

This is substantially below a theoretical value of 15×10^{-6} for the ^{234}U nucleus which was calculated recently by Marshalek[56] using the self-consistent cranking model for rotational nuclei. However, Kienle finds that Marshalek's values are consistently a factor of 3 to 7 times larger than experimental results.[1] The negative value indicates a shrinking of the nucleus in its excited state.

When the dispersion parameter is added to the least-squares fitting procedure, the experimental isomer shift changes. The value of κ as defined in Equation (35) is found to be 1.35 for the $^{238}PuO_2(r)$ run and 1.22 for the $^{238}PuAl_4(r)$ run. These values are slightly larger than those given by Wagner et al.[26] for E2 transitions in a variety of even-even nuclei. Since the absorber was the same for both runs, the dispersion parameters (which depend only on the absorber) should have the same value. For $^{238}PuO_2(r)$, $\xi = 0.025 \pm 0.002$ and for $^{238}PuAl_4(r)$, $\xi = 0.013 \pm 0.003$. These values do not agree, and seem too large for a transition whose gamma-ray energy falls below the K electron absorption edge.[26]

One explanation for this discrepancy might be abnormalities in the drive motion or alignment problems in the transducer armature. Another possibility is a quadrupole interaction in the source due to vacancies in the lattice or Frenkel defects caused by self-irradiation damage. The 48.31 mm/sec FWHM of the absorption lines obtained using the $^{238}PuO_2$(r) source would give an estimate of ∿22 mm/sec for the quadrupole coupling in the source. The magnitude of the electric field gradient at the Pu site would have to be ∿3 x 10^{18} V/cm^2 to produce such an interaction (see page 62). The 36.53 mm/sec FWHM of the absorption lines obtained using the $^{238}PuAl_4$(r) source would give an estimate of ∿15 mm/sec for the quadrupole coupling in the source. The magnitude of the electric field gradient at the Pu site would have to be ∿2 x 10^{18} V/cm^2.

The quadrupole interaction for a 2^+ to 0^+ gamma-ray transition is asymmetric about zero velocity (see Figure 3, page 16) and hence a quadrupole interaction in the source could cause an "apparent" dispersion in the Mössbauer absorption line. As predicted by Rand et al.[45] the number of Frenkel defects per unit cell should be larger for PuO_2 than for plutonium-aluminum alloys. Thus the electric field gradient produced by these defects should be larger for PuO_2 than for $PuAl_4$, since it will be partially screened by the conduction electrons in an alloy. The ratio of the dispersion parameters for the $^{238}PuO_2$(r) source and the $^{238}PuAl_4$(r) source is 1.91 ± 0.46 and the ratio of the estimated quadrupole coupling in the $^{238}PuO_2$(r) source and the $^{238}PuAl_4$(r) is about 1.5. The trend of these ratios agrees and would seem to indicate that a quadrupole interaction in the source may account for part or all of the "apparent" dispersion in the Mössbauer absorption line.

IV. CONCLUSIONS

The nuclear gamma resonance for ^{238}U, ^{236}U, and ^{234}U in the compound uranyl rubidium nitrate has been established at 4.2° K following the alpha decay of PuO_2 sources. The ratios of the quadrupole moments of these isotopes have been determined and the electric field gradient at the uranium site has been calculated. The hexadecapole interaction has been investigated in ^{234}U. A maximum value for the hexadecapole coupling parameter has been determined; however this leads to a third derivative of the electric field at the uranium nucleus which is three orders of magnitude too large, even allowing for a generous Sternheimer factor. The isomer shift in ^{234}U has been measured for both PuO_2 and $PuAl_4$ sources, and an estimate for the change in nuclear radius between the excited and ground states has been given. An attempt was made to determine the value of the dispersion parameter, but inconclusive results were obtained.

In order to investigate the "apparent" dispersion, a better drive system should be fabricated and a computer fit employed which takes into account the contribution in the gamma-ray window of the counts from the moving absorber. It would be interesting to investigate the isomer shifts for a variety of oxidation states of uranium and compare them with results found in Np[55] and Am.[30] If UCl_3 and U_2S_3 could be obtained, they would provide an oxidation state of (III) and the compound $K(UO_2)CO_3$ would provide an oxidation state of (V). In this way chemical properties of uranium compounds could be correlated with the experimental isomer shifts, and the systematics compared with those in other actinides.

LIST OF REFERENCES

LIST OF REFERENCES

1. J.A. Stone, in IAEA Technical Report Series No. 50, 179 (1966); P. Kienle, in Hyperfine Structure and Nuclear Radiations, edited by E. Matthias and D.A. Shirley, (North-Holland Publishing Company, Amsterdam, 1968), p. 27.

2. R.L. Mössbauer, Z. Physik 151, 125 (1958); Naturwissenschaften 45, 538 (1958).

3. H. Frauenfelder, The Mössbauer Effect, (W.A. Benjamin, New York, 1962); G.K. Wertheim, Mössbauer Effect: Principles and Applications, (Academic Press, New York, 1964).

4. D. Seyboth, F.E. Obenshain, and G. Czjzek, Phys. Rev. Letters 14, 954 (1965); Y.K. Lee, P.W. Keaton, Jr., E.T. Ritter, and J.C. Walker, Phys. Rev. Letters 14, 957 (1965).

5. J.R. Oleson, Y.K. Lee, J.C. Walker, and J.W. Wiggins, Phys. Letters 25B, 258 (1967); N. Hershkowitz, C.G. Jacobs, Jr., and K.A. Murphy, Phys. Letters 27B, 563 (1968).

6. J.A. Stone and W.L. Pillinger, Phys. Rev. Letters 13, 200 (1964).

7. D.A. Goldberg, Y.K. Lee, E.T. Ritter, R.R. Stevens, Jr., and J.C. Walker, Phys. Letters 20, 571 (1966); J.S. Eck, Y.K. Lee, J.C. Walker, and R.R. Stevens, Jr., Phys. Rev. 156, 246 (1967).

8. J.A. Monard, Paul G. Huray, and J.O. Thomson, Bull. Am. Phys. Soc. 17, 86 (1972).

9. Paul G. Huray, J.A. Monard, and J.O. Thomson, Oak Ridge National Laboratory Report No. ORNL-4743, 100 (1972).

10. S.L. Ruby, G.M. Kalvius, B.D. Dunlap, G.K. Shenoy, D. Cohen, M.B. Brodsky, and D.J. Lam, Phys. Rev. 184, 374 (1969); G.K. Shenoy, G.M. Kalvius, S.L. Ruby, B.D. Dunlap, M. Kuznietz, and F.P. Campos, Intern, J. Magnetism 1, 23 (1970).

11. R. Meeker, G.M. Kalvius, B.D. Dunlap, S.L. Ruby, and D. Cohen, Bull. Am. Phys. Soc. 17, 85 (1972).

12. G.T. Trammell and J.P. Hannon, Phys. Rev. 180, 337 (1969).

13. G. Raphael and R. Lallement, Solid State Commun. 6, 383 (1968); M.C. Gregory, private communication; J.C. Eisenstein and M.H.L. Pryce, Proc. Roy. Soc. (London), A229, 20 (1955); S.P. McGlynn and J.K. Smith, J. Mol. Spectry. 6, 164 (1961).

14. E.A.C. Lucken, Nuclear Quadrupole Coupling Constants, (Academic Press, London, 1969).

15. R.L. Mössbauer, Lectures prepared by M.J. Clauser, in Hyperfine Interactions, edited by A.J. Freeman and R.B. Frankel, (Academic Press, New York, 1967), p. 497.

16. Tien-Chuan Wang, Phys. Rev. 99, 566 (1955).

17. R.J. Mahler and L.W. James, Phys. Rev. Letters 16, 259 (1966); in Magnetic Resonance and Relaxation, edited by R. Blinc, (North-Holland Publishing Company, Amsterdam, 1967), p. 938.

18. M.E. Rose, Elementary Theory of Angular Momentum, (John Wiley and Sons, Inc., New York, 1957).

19. R.R. Roy and B.P. Nigam, Nuclear Physics: Theory and Experiment, (John Wiley and Sons, Inc., New York, 1967).

20. H. Frauenfelder and R.M. Steffen, in Alpha-, Beta-, and Gamma-Ray Spectroscopy, edited by K. Siegbahn, (North-Holland Publishing Company, Amsterdam, 1965), Vol. II, p. 997.

21. S.V. Karyagin, Doklady Akad. Nauk SSSR 148, 1102 (1963); V.I. Gol'danskii, E.F. Makarov, and V.V. Khrapov, Phys. Letters 3, 334 (1963); V.I. Gol'danskii, The Mössbauer Effect and Its Application to Chemistry, (D. Van Nostrand Co., Inc., New York, 1966); V.I. Gol'danskii, S.V. Karyagin, E.F. Makarov, and V.V. Khrapov, in Transactions of the Conference on the Mössbauer Effect, (Dubna, July 1962).

22. D.A. Shirley, Rev. Mod. Phys. 36, 339 (1964).

23. T.C. Tucker, L.D. Roberts, C.W. Nestor, Jr., T.A. Carlson, and F.B. Malik, Phys. Rev. 178, 998 (1969).

24. Yu. Kagan, A.M. Afanas'ev, and V.K. Voitovetskii, ZhETF Pis. Red. 9, 155, (1969); C. Sauer, E. Matthias, and R.L. Mössbauer, Phys. Rev. Letters 21, 961 (1968).

25. J.P. Hannon and G.T. Trammell, Phys. Rev. Letters 21, 726 (1968).

26. J.P. Hannon and G.T. Trammell, Phys. Rev. 186, 306 (1969).

27. F.E. Wagner, B.D. Dunlap, G.M. Kalvius, H. Schaller, R. Felsher, and H. Spieler, Phys. Rev. Letters 28, 530 (1972).

28. A.M. Afanas'ev and Yu. Kagan, Phys. Letters 31A, 38 (1970).

29. C.E. Haynes, private communication.

30. M.C. Gregory, R.W. Lougheed, and E.K. Hulet, Bull. Am. Phys. Soc. 17, 546 (1972); M.C. Gregory, private communication.

31. H.L. Adair, J. Inorg. Nucl. Chem. 32, 1173 (1970).

32. J.W.T. Dabbs, L.D. Roberts, and G.W. Parker, Physica 24, S69 (1958); L.D. Roberts, J.W.T. Dabbs, and G.W. Parker, Proc. 2nd UN Int. Conf. PUAE 15, 322 (1958); L.D. Roberts, J.W.T. Dabbs, F.J. Walter, S.H. Hanauer, and G.W. Parker, in Radioisotopes in the Physical Sciences and Industry, (IAEA, Vienna, 1962), Vol. 1, p. 329.

33. M.A. Stroscio, D.J. Erickson, and L.D. Roberts, Bull. Am. Phys. Soc. 15, 198 (1970); L.D. Roberts, private communication.

34. T.J. Kirthlink, Jr., thesis, University of Tennessee, 1971 (unpublished).

35. R.S. Preston, S.S. Hanna, and J. Heberle, Phys. Rev. 128, 2207 (1962).

36. R.H. Herber and R.G. Hayter, J. Am. Chem. Soc. 86, 301 (1964).

37. John Burton, Oak Ridge National Laboratory Report No. ORNL-4743, 105 (1972).

38. Anthony Ralson, A First Course in Numerical Analysis, (McGraw-Hill, New York, 1965).

39. J.L. Hoard and J.P. Stroupe, quoted by G.H. Dieke and A.B.F. Duncan, in Spectroscopic Properties of Uranium Compounds, (National Nuclear Energy Series III-2, McGraw-Hill, New York, 1949), p. 15.

40. W.H. Zachariasen, Acta. Cryst. 7, 795 (1954).

41. J.I. Bullock, J. Chem. Soc. (A), 781 (1969).

42. G.A. Barclay, T.M. Sabine, and J.C. Taylor, Acta Cryst. 19, 205 (1965).

43. F.S. Galasso, Structure and Properties of Inorganic Solids, (Pergammon Press, Oxford, 1970).

44. L.B. Asprey, F.H. Ellinger, S. Fried, and W.H. Zachariasen, J. Am. Chem. Soc. 77, 1707 (1955).

45. M.H. Rand, A.C. Fox, and R.S. Street, Nature 195, 567 (1962).

46. K. Mendelssohn, E. King, J.A. Lee, M.H. Rand, C.S. Griffin, and R.S. Street, in Plutonium 1965, edited by A.E. Kay and M.B. Waldron, (Chapman and Hall, Ltd., London, 1967), p. 189.

47. G.M. Kinchin and R.S. Pease, Rep. Prog. Phys. 18, 1 (1955).

48. B.S. Borie, Jr., Trans. AIME 191, 800 (1951).

49. O.J.C. Runnalls, in Plutonium 1965, edited by A.E. Kay and M.B. Waldron, (Chapman and Hall, Ltd., London, 1967), p. 341.

50. F.H. Ellinger, C.C. Land, and W.N. Miner, J. Nucl. Mat. 5, 165 (1962).

51. J.L.C. Ford, Jr., P.H. Stelson, C.E. Bemis, Jr., F.K. McGowan, R.L. Robinson, and W.T. Milner, Phys. Rev. Letters 27, 1232 (1971).

52. L.D. Roberts and J.W.T. Dabbs, Oak Ridge National Laboratory Report No. ORNL-2910, 62 (1960).

53. C.E. Bemis, Jr., private communication.

54. R.M. Sternheimer, Phys. Rev. Letters 6, 190 (1961); Phys. Rev. 123, 870 (1961); Phys. Rev. 146, 140 (1966).

55. W.L. Pillinger and J.A. Stone, in Mössbauer Effect Methodology, edited by I.J. Gruverman, (Plenum Press, New York, 1968), p. 217.

56. E.R. Marshalek, Phys. Rev. Letters 20, 214 (1968).

APPENDICES

APPENDIX A

HIGH-VELOCITY COIL

An electromechanical pickup coil has been designed which consists of a set of coils in cylindrical geometry surrounding a bar magnet on the cylinder axis. The bar magnet is mounted on the armature of the transducer. The electromotive force due to motions normal to the axis of symmetry of the coil has been calculated to be less than one part in 10^5. The electromotive force of the solenoid is also calculated to be directly proportional to the velocity of the magnet (to within one part in 10^5) over a range of magnet positions of one millimeter.

Two coils have been designed: one for high velocities and one for low velocities. A general coilform is shown in Figure 20. The dimensions which differ for the high- and low-velocity coils are given in Table IX. The number of turns designed to be wound on each coil shim (A) and each coil (B) is listed in Table X. It is the high-velocity coil which was used in this work. The most important part of the design is the ratio of total turns per coil to total turns per coil shim (990:190 or 5.2105:1). In practice, it is very difficult to achieve the designed windings for each coil and shim. The actual windings of the high-velocity coil used in this work are given in Table XI. The ratio of total turns per coil to total turns per coil shim is 966:185 or 5.2216:1, a difference of 0.2% from the designed ratio. Extra turns had to be added to the last layer of the coil shims to achieve the designed ratio. An Alnico bar magnet 1.600 ± 0.005 in. in length and 0.315 ± 0.001 in. in diameter was used with the coil.

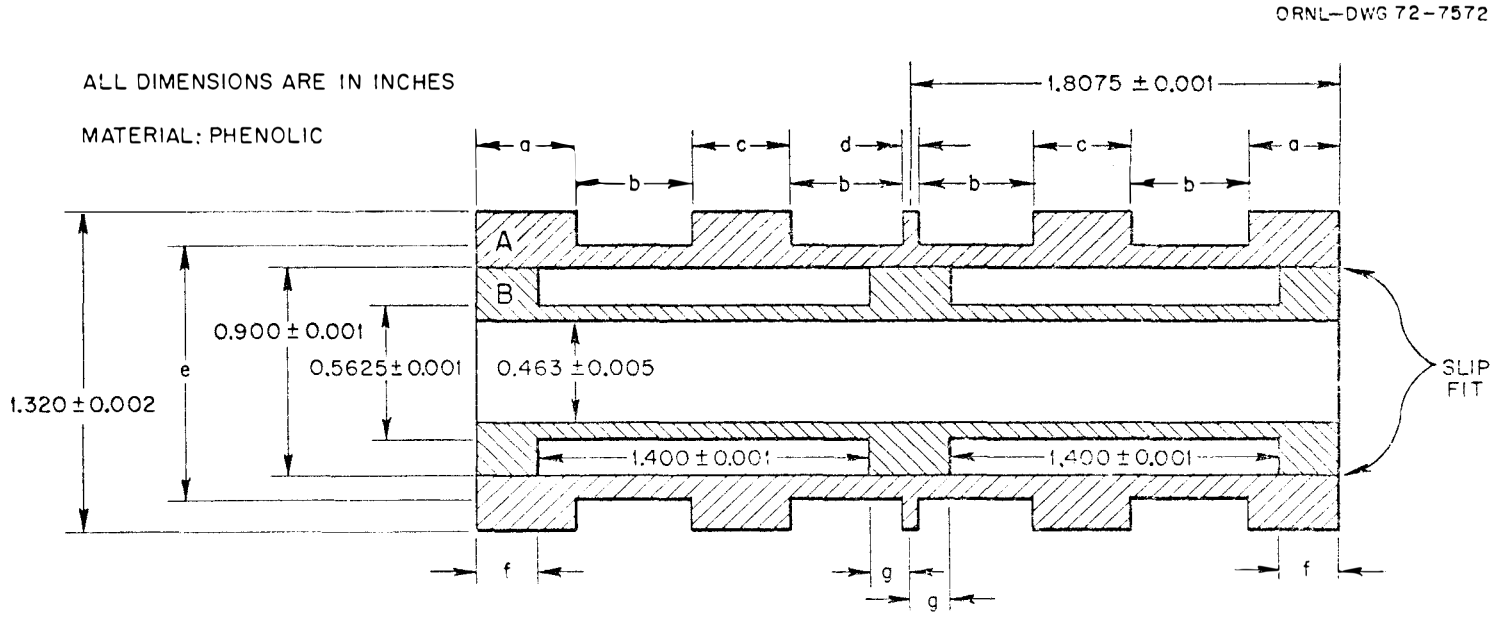

Velocity Coil Designed for Radial Velocity Pickup <1 Part in 10^5 and Nonlinearity <1 Part in 10^5.

Figure 20. Schematic of the velocity coilform.

Table IX

Velocity Coil Dimensions*

Coilform	Section	Low-Velocity Coil	High-Velocity Coil
A	a	0.3875 ± 0.001	0.3865 ± 0.001
	b	0.500 ± 0.001	0.260 ± 0.001
	c	0.400 ± 0.001	0.880 ± 0.001
	d	0.040 ± 0.001	0.042 ± 0.001
A	e	1.050 ± 0.001	1.160 ± 0.001
B	f	0.245 ± 0.001	0.2495 ± 0.001
B	g	0.1625 ± 0.001	0.158 ± 0.001

*All dimensions are in inches.

Table X

Velocity Coil Windings*

Coilform		Number of Layers/Coil	Number of Turns/Layer	Total Turns	Comments
A	Low-velocity	13	78-81	1040	Layer of paper after every fourth layer of wire
B	Low-velocity	19	223-225	4256	Layer of paper after each layer of wire
A	High-velocity	4	46-48	190	
B	High-velocity	4	247-249	990	

*No. 36 B&S copper wire to be used for all coils.

Table XI

Actual Windings for High-Velocity Coil*

Coilform	First Layer (turns)	Second Layer (turns)	Third Layer (turns)	Fourth Layer (turns)	Total (turns)
A	45	44	43	46+7	185
A	45	44	43	44+9	185
A	45	44	44	44+8	185
A	45	44	44	44+8	185
B	242	241	241	242	966
B	242	242	242	240	966

*No. 36 B&S copper wire used for all coils.

APPENDIX B

FOURIER ANALYSIS OF CALIBRATION SPECTRA

```
      SUBROUTINE FFT(M,A,CK,CS)
C
C THIS SUBROUTINE ANALYZES THE HARMONIC CONTENT OF THE
C   POINT BY POINT CALIBRATION OF THE VELOCITY WAVEFORM
C
C SUBROUTINE AUTHOR M. R. PATTERSON
C   COMPUTING TECHNOLOGY CENTER, ORNL
C
C FFT SUBROUTINE TO BE USED WITH PROGRAM SINFIT
C   WRITTEN BY J. A. MONARD FOR INPUT/OUTPUT
C
C       CK=0     GENERATE TABLE OF CS(I) ONLY
C          1,-1 GEN. TABLE AND TRANSFORM(1), INVERSE(-1)
C          2,-2 ASSUME TABLE, GEN. TRAN.(2), INV(-2)
C
      INTEGER*4 CK
      REAL*4 CS(1)
      DATA PI/3.141593E0/
      COMPLEX*8 A(1),W,T
      IC=CK
      IF (IABS(IC).GT.1) GO TO 20
C           GENERATE TABLE OF COSINES, ETC.
      IF(M.LE.0) CALL EXIT
      MOLD=M
      FNM=NM
      NM=2**M
      NMT=NM/2
      NMTP1=NMT+1
      NMF=NMT/2
      NMFP1=NMF+1
      FNMT=NMT
      PION=PI/FNMT
      DO 10 I=1,NMFP1
         FI=I-1
         THT=FI*PION
   10    CS(I)=COS(THT)
      IF (IC.EQ.0) GO TO 140
   20 IF (M.NE.MOLD) CALL EXIT
      IF (IC.GT.0) GO TO 40
C           INVERSE=(TRANSFORM(A*)/N)*, THUS CONJUGATE
      DO 30 I=1,NM
   30    A(I)=CONJG(A(I))
C           TRANSFORM
   40 DO 100 L=1,M
C
```

```
      LP1=L+1
      MML=M-L
      NSTEP=2**MML
      NS2=2*NSTEP
      ITER=NM/NS2
      DO 90 J=1,ITER
C       THE LAST BIT SHOULD ALWAYS BE ZERO FOR IR
        IR=(J-1)*2
        IBR=0
        DO 50 IL=1,L
          K=MOD(IR,2)
          IBR=2*IBR+K
          IR=IR/2
   50     CONTINUE
        IBR=IBR*NSTEP
        IBI=IABS(NMF-IBR)+1
        WI=CS(IBI)
        IF (IBR.GT.NMF) GO TO 60
        WR=CS(IBR+1)
        GO TO 70
   60   WR=-CS(NMTP1-IBR)
   70   W=CMPLX(WR,WI)
        NB=(J-1)*NS2
        DO 80 I=1,NSTEP
          N=NB+I
          N1=N+NSTEP
          T=A(N1)*W
          A(N1)=A(N)-T
          A(N)=A(N)+T
   80     CONTINUE
   90   CONTINUE
  100 CONTINUE
C       THE FOURIER SUMS ARE COMPLETE, BUT THEIR
C       ADDRESSES ARE BIT-REVERSED. THE FOLLOWING
C       CODING PUTS THEM IN ORDER.
      DO 120 I=1,NM
        IR=I-1
        IBR=0
        DO 110 J=1,M
          K=MOD(IR,2)
          IBR=2*IBR+K
          IR=IR/2
  110     CONTINUE
C       IBR IS THE BIT-REVERSED VALUE OF I-1
        IBR=IBR+1
        IF (IBR.LE.I) GO TO 120
        T=A(I)
C
```

```
          A(I)=A(IBR)
          A(IBR)=T
  120     CONTINUE
C           BIT REVERSAL IS COMPLETE
        IF (IC.GT.0) GO TO 140
C           CONJUGATE AND DIVIDE BY N
        DO 130 I=1,NM
  130     A(I)=CONJG(A(I))/FNM
  140 RETURN
        END
```

APPENDIX C

CONVERSION FROM CHANNELS TO VELOCITY

```
      SUBROUTINE INPUTS
C
C THIS SUBROUTINE CONVERTS CHANNEL INFORMATION TO VELOCITY
C   INFORMATION USING A POINT BY POINT CALIBRATION OF THE
C     VELOCITY WAVEFORM
C
C INPUTS SUBROUTINE TO BE USED WITH PROGRAM LSFMTI
C   WRITTEN BY JOHN BURTON
C
C SUBROUTINE AUTHOR J. A. MONARD
C   PHYSICS DIVISION, ORNL
C
      IMPLICIT REAL*8(A-H),REAL*8(O-Z)
      COMMON /BLK5/AO,ES(1025),AC(1025),A(1025),ER(1025),
     1  ER2(1025),NDP
      COMMON /BLK8/ESS(1025),EFOLD
      COMMON /BLK9/PHASE,COP,VMAX,NM
      DIMENSION IFM(20)
      DIMENSION CAL(1025)
      PI = 3.14159265358979D0
C
C IFM IS THE FORMAT OF THE INPUT DATA
C NM INDICATES THE NUMBER OF MILLIONS OVERFLOW
C COP INDICATES THE OVERFLOW CUT OFF POINT
C VMAX IS THE MAXIMUM VELOCITY OF THE SINE WAVE IN MM/SEC
C IF VMAX EQUALS ZERO ONLY CHANNEL INFORMATION IS USED
C
      READ (50,1000) IFM
 1000 FORMAT (20A4)
      READ (50,2000) NM, COP, VMAX
 2000 FORMAT (I10,2F10.0)
C
C NDP IS THE NUMBER OF DATA POINTS AND MUST NOT EXCEED 1025
C A(I) IS THE ARRAY OF EXPERIMENTAL AMPLITUDES OF THE
C   MOESSBAUER SPECTRUM
C CAL(I) IS THE ARRAY OF EXPERIMENTAL AMPLITUDES OF THE
C   VELOCITY WAVEFORM
C
      READ (50,IFM) (A(I),I=1,NDP)
      READ (50,IFM) (CAL(I),I=1,NDP)
C
C CALMAX IS THE MAXIMUM AMPLITUDE OF THE VELOCITY WAVEFORM
C CALMIN IS THE MINIMUM AMPLITUDE OF THE VELOCITY WAVEFORM
C CALAVG IS THE AVERAGE AMPLITUDE OF THE VELOCITY WAVEFORM
C
```

```
      CALMAX = 0.25*(CAL(1)+CAL(2)+CAL(NDP)+CAL(NDP-1))
      CALMIN = 0.25*(CAL(NDP/2-1)+CAL(NDP/2)+CAL(NDP/2+1)+
     1  CAL(NDP/2+2))
      CALAVG = 0.0
      DO 10 I=1,NDP
   10 CALAVG = CALAVG+CAL(I)
      CALAVG = CALAVG/DFLOAT(NDP)
      CALCON = (2.0*VMAX)/(CALMAX-CALMIN)
      IF (CALMAX.LT.CALMIN) CALCON = -CALCON
      DO 60 I=1,NDP
      IF (NM) 40,40,20
   20 IF (A(I).LT.COP) GO TO 30
      A(I) = (NM-1)*1.E6+A(I)
      GO TO 40
   30 A(I) = NM*1.E6+A(I)
C
C  ES(I) IS THE ARRAY OF VELOCITY OR CHANNEL INFORMATION
C  ER(I) IS THE ARRAY OF STATISTICAL ERRORS
C
   40 IF (VMAX.LT.1.E-10) GO TO 50
      ES(I) = -CALCON*(CALAVG-CAL(I))
      GO TO 60
   50 ES(I) = DFLOAT(I)-1.
   60 ER(I) = DSQRT(A(I))
      RETURN
      END
```

VITA

Joyce Anne Monard was born in Bethlehem, Pennsylvania on November 5, 1946. Her elementary education was obtained in various schools in Connecticut, Illinois, and New Jersey, and she graduated first in her class from Trenton Central High School in 1964. In May, 1968, she graduated summa cum laude with honors from Bryn Mawr College in Bryn Mawr, Pennsylvania with a Bachelor of Arts in physics. During her undergraduate work, she was awarded the Maria L. Eastman Brooke Hall Memorial Scholarship, the Charles S. Hinchman Memorial Scholarship, and the Bryn Mawr European Fellowship. She joined the staff of the Thermonuclear Division at the Oak Ridge National Laboratory for a period of three months immediately following graduation. In September of 1968 she accepted a National Science Foundation Traineeship at The University of Tennessee in Knoxville and began working toward a Ph.D degree in physics. In February of 1970 she started her dissertation research on campus and in July of 1971 moved her experiment to the Transuranium Research Laboratory at the Oak Ridge National Laboratory. In February, 1972 she gave a talk on her doctoral research at the American Physical Society meeting in San Francisco, California.